Reynolds number dependence of the structure functions in homogeneous turbulence

John Kaminsky[1], Björn Birnir[1,3], Gregory P. Bewley[2],
and Michael Sinhuber[4]

CNLS and Department of Mathematics
UC Santa Barbara[1], University of Iceland[3],
Department of Mechanical Engineering
Cornell University[2], and
Department of Civil and Enviromental Engineering
Stanford University[4].

Abstract

We compare the predictions of stochastic closure theory (SCT) [6] with experimental measurements of homogeneous turbulence made in the Variable Density Turbulence Tunnel (VDTT) [10] at the Max Planck Institute for Dynamics and Self-Organization in Göttingen. While the general form of SCT contains infinitely many free parameters, the data permit us to reduce the number to seven, only three of which are active over the entire inertial range. Of these three, one parameter characterizes the variance of the mean field noise in SCT and another characterizes the rate in the large deviations of the mean. The third parameter is the decay exponent of the Fourier variables in the Fourier expansion of the noise, which characterizes the smoothness of the turbulent velocity.

SCT compares favorably with velocity structure functions measured in the experiment. We considered even-order structure functions ranging in order from two to eight as well as the third-order structure functions at five Taylor-Reynolds numbers (R_λ) between 110 and 1450. The comparisons highlight several advantages of the SCT, which include explicit predictions for the structure functions at any scale and for any Reynolds number. We observed that finite-R_λ corrections, for instance, are important even at the highest Reynolds numbers produced in the experiments.

SCT gives us the correct basis function to express all the moments of the velocity differences in turbulence in Fourier space. These turn out to be powers of the sine function indexed by the wavenumbers. Here, the power of the sine function is the same as the order of the moment of the velocity differences (structure functions). The SCT produces the coefficients of the series and so determines the statistical quantities that characterize the small scales in turbulence. It also characterizes the random force acting on the fluid in the stochastic Navier-Stokes equation, as described in the paper.

1 Introduction

Let us begin with a brief history of wind tunnel research and of the effort to describe the structure of turbulence statistically. In Aeronautics, the design of airfoils and airplanes was a major challenge. The development of appropriate laboratory experiments facilitates progress to this day, including the invention of the wind tunnel. The first wind tunnel is credited to F. Wenham in Great Britain in 1871. The Wright brothers also constructed their own wind tunnel in 1901 [2], but it was Ludwig Prandtl in 1917 who designed the first "modern" wind tunnel. This 1917 tunnel was actually his second design, his first design in 1909 being a closed-loop wind tunnel which, by his own admission, was "of a temporary nature" [24]. Nonetheless, his second, more permanent design would become the model for many subsequent wind tunnels [1]. Prandtl's student, Max Munk, went on to design the first wind tunnel that allowed adjustment of the density of the working fluid [10], and so for much higher Reynolds number flows in the tunnel. This tunnel was built at the Langley Research Center in Virgina in 1923. Most of the early research done with wind tunnels was devoted to the study of airfoils and airplane shapes and Mach number [10]. One interesting feature of these tunnels was the ability to adjust Mach number and Reynolds number independently.

Wind tunnels are essential tools to study not only airfoils and model airplanes, but also to study statistically homogeneous and isotropic turbulence, see Taylor [30]. Such flows limit turbulence to its essential ingredients: inertia, pressure and friction, minimize the effects of the boundaries on the flow, and do not exhibit a preferred orientation. It can be created by mechanically stirring a liquid or gas [10]. A close approximation of such flows are realized in a wind tunnel when a uniform free-stream flow is disturbed by a mesh or a grid, see [12, 11].

Experiments to study turbulence were rare until the second half of the twentieth century. The 1940s featured experiments on grid turbulence in California

[21], while another series of experiments were performed at the Nuclear Research Lab in Jülich in the 1970s [16]. More recently, wind tunnels were built at the German Aerospace Center in Göttingen and at the Princeton Gas Dynamics Lab with similar goals. The experiments in this paper were performed in the facility at the Max Planck Institute for Dynamics and Self-Organization in Göttingen called the Variable Density Turbulence Tunnel (VDTT), which was completed in 2009 [10]. It has achieved turbulent flow up to Taylor-Reynolds number 1600, which is the highest recorded for a passive grid experiment until that time, with higher Reynolds number since being recorded with an active grid[29, 28]. Details about the VDTT can be found in [10]. One of Prandtl's original wind tunnels sits beside the VDTT in Göttingen, see [10].

The mathematical theory of turbulence has its roots in the work of Kolmogorov. In 1941, Kolmogorov published his celebrated four-fifths law and postulated, with Obukhov, that the structure functions of turbulence should scale with the lag variable, r, so that

$$S_p(x,y,t) = E(|u(x,t) - u(y,t)|^p) = C_p \, r^{p/3},$$

where p is the order of the structure function and $r = |x - y|$. Lev Landau criticized the theory for neither taking into account the organization of the flow on large scales nor the influence of intermittency, which is the development of long tails in the velocity difference distributions at large Reynolds numbers. In 1962, Kolmogorov and Obukhov revised their theory to address these criticisms. They introduced a correction to the exponent, such that

$$S_p(x,y,t) = C_p < \varepsilon^{\frac{p}{3}} > r^{\frac{p}{3}} = C_p' r^{\frac{p}{3}+\tau_p} = C_p' r^{\zeta_p},$$

where ε is the dissipation rate and $\zeta_p = \frac{p}{3} + \tau_p$, and τ_p is the correction that needs to be determined. A prediction for the correction was found by She and Leveque in 1994:

$$\tau_p = -\frac{2p}{9} + 2(1 - (\frac{2}{3})^{\frac{p}{3}}), \tag{1}$$

see [26]. In [6], the log-Possonian processes of Dubrulle [14] and She and Waymire [27], responsible for the intermittency corrections, were derived from the stochastic Navier-Stokes equation.

Kolmogorov and Obukhov considered the velocity in turbulent flow to be a stochastic process and their hypotheses include that the N-point probability distribution function (PDF) of turbulence does not depend on x or y individually but

3

only on r, ν and ε, where r is the lag variable, ν is the kinematic viscosity, and ε is the kinetic energy dissipation rate of the turbulence per unit mass [23]. Moreover, when $r >> \eta$, where η is the Kolmogorov (or dissipation) scale, then the PDF depends on ε and r alone, and not on ν. Since the 2-point PDF determines the structure functions described above, the same statements that apply to the PDFs apply also to the structure functions.

If the turbulent velocity is a stochastic process it must satisfy a stochastic Navier-Stokes equation. Such an equation was formulated by Landau and Lifschitz in their Fluid Dynamics book [20] in 1959. They considered the noise in the stochastic Navier-Stokes equation to be the fluctuations in the velocity, which cannot be ignored in turbulence. They argued that it should be white both in time and space, but this assumption cannot be true since the Navier-Stokes equation driven by noise that is white in space produces velocities the are not continuous [32], and this is not observed in nature. Birnir [6] argued that the noise has enough smoothness in space that the dissipation rate, ε, is finite, and that the noise is of a generic nature that includes an additive term corresponding to a mean-field noise and another additive term corresponding to the large deviations of the mean-field. He also added a multiplicative noise term, modeling jumps in the gradient for the flow velocity, and showed that this term produced the log-Poisson process of Dubrulle, She and Waymire and their intermittency corrections τ_p. These assumptions are the basis of the Stochastic Closure Theory (SCT) [7] and are elaborated in the next section.

2 The Assumptions of SCT and Its Predictions

The following assumptions produce the Stochastic Navier-Stokes equation (7) given in the next section. The detailed arguments leading to the form of the noise are given in [6] and [7]. They follow the spirit of the argument in Landau and Lifschitz [20]. We also list the predictions of the theory, which include a quantitative prediction of the She-Leveque intermittency corrections to the Kolmogorov-Obukhov '62 theory of turbulence.

SCT Assumptions:

1. The small scale flow in fully developed turbulence satisfies a stochastic Navier-Stokes (SNS) equation.

2. The noise in the SNS consists of both an additive and a multiplicative term.

3. The additive noise is in part a general mean field noise that is sufficiently smooth in space for the dissipation rate,

$$\varepsilon = v \int_{\Omega} |\nabla u|^2 dx < \infty,$$

   to be finite. In addition to this "infinite-dimensional Brownian" mean-field noise, there is a deterministic additive part that captures large-deviations in the mean-field.

4. The multiplicative noise models jumps in the velocity gradient, ∇u. This term is then multiplied by the velocity u.

5. The most singular (having least spatial smoothness) structures in (3-d) turbulence are one-dimensional vortex lines.

SCT Predictions:

1. The structure functions of turbulence at finite Reynolds numbers are given by formulas that explicitly incorporate the Reynolds number dependence of the structure functions.

2. The N-point probability density function exists and can be computed. In the two-point case it is determined by the Kolmogorov-Hopf functional differential equation [7] and has an explicit formula [8].

3. The PDF for the velocity distribution in turbulence is a Generalized-Hyperbolic distribution [3] convolved with the Poisson distribution of the log-Poisson processes of Dubrulle, She and Waymire [8]. For large values of the lag variable and for the fluid velocities themselves, these distributions become (skewed and flat) Gaussians.

The most important SCT prediction for this paper is (1), the explicit formulae for the structure functions with given Reynolds number dependencies. We use these formulas to fit the data measured in the VDTT, and this is the subject of the paper. A disadvantage of equation is that the noise has infinitely many undetermined coefficients c_k, d_k and h_k. The last coefficients are a consequence of assumption 3 above. The vorticity lines are one-dimensional, and this implies that all the coefficients, h_k, are fixed [7]. However, we are still left with infinitely many coefficients c_k and d_k. What we find through comparison with the experimental data is that we can reduce the number of coefficients to only three. When the

5

mean flow is given, we are left with one parameter that characterizes the infinite-dimensional Brownian, another parameter characterizing large deviations from the mean, and one exponent characterizing spatial smoothness. We find, as expected, that the mean flow and the three parameters depend on the Taylor-Reynolds number. They do not, however, depend on the order of the structure function. The upshot is a much improved stochastic closure model (25) with only three parameters characterizing the noise.

One can say that the SCT produces the correct basis, with basis functions that are functions of the lag variable indexed by the wavenumber, to represent all the statistical quantities of the velocity differences. This is a big improvement over previous theoretical result that only produce one or finitely many statistical quantities measurable in experiments.

3 The Stochastic Closure Model

In this section, we give a short derivation of the SCT model. We first explain how the form of the turbulent noise forcing, in the Navier-Stokes equation, is derived and then use some techniques from probability theory to transform the resulting stochastic Navier-Stokes equation, for the small scale velocity, to an integral equation. The integral equation will be used in the next section to compute a sharp lower estimate for the structure functions. The reader is directed to [7] for more details.

The flow in the wind tunnel is governed by the Navier Stokes equation:

$$u_t + (u \cdot \nabla)u = \nu \Delta u - \nabla p,$$
$$\operatorname{div} u = 0, \qquad (2)$$
$$u(x,0) = u_0(x),$$

where $u(x)$ is the fluid velocity, $x \in \mathbb{R}^3$, p is pressure, and ν is the viscosity. We also impose periodic boundary conditions upon the flow. The second line in (2) is the incompressibility condition. Using this equation, we can eliminate the pressure to get

$$u_t + u \cdot \nabla u = \nu \Delta u + \nabla(\Delta^{-1}[\operatorname{Trace}(\nabla u)]^2). \qquad (3)$$

This equation defines the evolution of the velocity of the fluid in time. We will impose periodic boundary conditions on the small scales below.

6

Following the classical Reynolds decomposition [25], we decompose the velocity into mean flow U and the fluctuations u. Then the velocity is written as $U + u$, where U describes the mean, or large scale flow and u describes the velocity fluctuations. These two terms describe the large scales and small scales of the flow, respectively. If we also decompose the pressure into mean pressure P and the fluctuations p, then the equation for the large scale flow can be written as

$$U_t + U \cdot \nabla U = \nu \Delta U - \nabla P - \nabla \cdot (\overline{u \otimes u}), \tag{4}$$

where in coordinates

$$\nabla \cdot (\overline{u \otimes u}) = \frac{\partial \overline{u_i u_j}}{\partial x_j},$$

that is ∇ is dotted with the rows of $\overline{u_i u_j}$, and $R_{ij} = \overline{u \otimes u}$ is the Reynolds stress, see [4]. The Reynolds stress has the interpretation of a turbulent momentum flux and the last term in (4) is also know as the eddy viscosity. It describes how the small scales influence the large scales. In addition, from linearity, we get divergence free conditions for U, and u

$$\nabla \cdot U = 0, \qquad \nabla \cdot u = 0.$$

Together, (4) and the divergence free condition on U give the Reynolds Averaged Navier-Stokes (RANS) that forms the basis for most contemporary simulations of turbulent flow. The large scale equation (4) is satisfied by the mean flow $U = $ constant in the measurement region of the VDTT. Thus in our case (4) reduces to the pressure gradient balancing the eddy viscosity.

Finding a constitutive law for the Reynolds stress $\overline{u \otimes u}$ is the famous closure problem in turbulence and we will solve that by writing down a stochastic equation for the small scale velocity u. This was first done by Landau and Lifschitz in [20].

The consequence of the SCT hypothesis is that the fluctuating velocity u in turbulence is a stochastic process that is determined by a stochastic partial differential equation (SPDE). It will be the Navier-Stokes equation for the fluctuations driven by noise, see below. This is the point of view taken by Kolmogorov in [18, 17, 19], but the question we have to answer is: what is the form of the noise? There is a wide array of literature on this question, trying to trace the form of the noise back to the fluid instabilities, but these attempts have proven to be unsuccessful. Any memory of the fluid instabilities is quickly forgotten in fully-developed turbulence and the noise seems to be of a general form. Thus it makes sense to try to put generic noise into the Navier-Stokes equations and see how the

7

Navier-Stokes evolution colors generic noise. Below we will answer what generic noise in the Navier-Stokes equation must look like, see [7] for more details.

For fully developed turbulence, we close the model with a stochastic forcing term to account for the small scales in (2) and (3). This noise term models the dissipation in the flow. We impose periodic boundary conditions and then discretize on the torus. Let p_k denote the dissipation process in the j-th box. We assume these dissipation processes in the flow are weakly coupled and have mean m. Thus, the average is given by

$$M_n = \frac{1}{n} \sum_{j=1}^{n} p_j.$$

We now make use of the Central Limit Theorem, which implies M_n will converge to a Gaussian distribution with mean zero and variance one. For the statement and proof of the Central Limit Theorem, see page 194 in [15]. Then, define

$$x_t^n = \frac{S_{[tn]} - nm}{\sqrt{n}\sigma},$$

where $S_n = \sum_{j=1}^{n} p_j$ and $[tn]$ denotes integer value. We now apply the Functional Central Limit Theorem, as given by Theorem 8.1 in [5], and so the processes x_t^n must converge in distribution to a Brownian motion b_t as $n \to \infty$. This must occur in the direction of any Fourier component and so we get

$$\bar{D} = \sum_{k \neq 0} c_k^{\frac{1}{2}} db_t^k e_k(x),$$

where $e_k(x) = e^{2\pi i k x}$ are distinct Fourier compoents complete with its own Brownian motion b_t^k, and $c_k^{\frac{1}{2}}$ are coefficients that converge sufficiently fast to ensure convergence of the entire series, see [7].

However, we also must measure the fluctuations in the dissipation which can be explained via the Large Deviation Principle. To apply the Large Deviation Principle, we need to describe the rate function associated with the process, which depends on whether the fluctuations are random. If they are, the fluctuations can be modeled by a Poisson process with rate λ and furthermore, if there is bias in the fluctuations, then the deviations of M_n are bounded above by a constant determining the direction of the bias times the rate η. Cramer's Theorem, see [7], then gives that the rate function is bounded by $\eta = \lambda$, and so the second additive noise terms is

$$D' = \sum_{k \neq 0} d_k \eta_k dt e_k(x).$$

8

Here, $e_k(x)$ is defined as above, d_k is defined similarly to $c_k^{0.5}$, and η_k are the rates in the k-th direction. We choose $\eta_k = |k|^{\frac{1}{3}}$ to line up with the scaling of the Central Limit Theorem term. Thus, the Large Deviation Principle gives the term

$$D' = \sum_{k \neq 0} d_k |k|^{\frac{1}{3}} dt e_k(x).$$

These two terms defined the additive noise forcing term. A more detailed description of these terms is given in [7].

A final forcing term comes from the multiplicative noise. This noise models jumps in the velocity gradient or vorticity concentrations. If we let N_t^k denote the number of velocity jumps associated to the k-th wave number that have occured by time t. This in turn implies that the differential

$$dN^k(t) = N^k(t+dt) - N^k(t)$$

denotes the number of jumps in the time interval $(t, t+dt]$. The multiplicative noise then has the form

$$J = \sum_{k \neq 0} \int_{\mathbb{R}} h_k(t, z) \bar{N}^k(dt, dz),$$

where h_k measures the size of the jump and $\bar{N}^k$ is the compensated number of jumps. For more information on the multiplicative noise, see [7].

Thus, adding the terms $\bar{D}$, D' and, J multiplied by u, to the Navier-Stokes equation, we get a stochastic PDE describing the fully developed turbulent small-scale flow in the wind tunnel:

$$
\begin{aligned}
du + u \cdot \nabla u \, dt = {} & [\nu \Delta u + \nabla(\Delta^{-1}[\text{Trace}(\nabla u)]) - u \cdot \nabla U - U \cdot \nabla u] dt \\
& + \sum_{k \neq 0} d_k |k|^{\frac{1}{3}} dt e_k(x) + \sum_{k \neq 0} c_k^{\frac{1}{2}} db_t^k e_k(x) \qquad (5) \\
& + u \sum_{k \neq 0} \int_{\mathbb{R}} h_k(t, z) \bar{N}^k(dt, dz).
\end{aligned}
$$

We drop the term $-u \cdot \nabla U$, in the equation above, since the mean flow U is constant for homogeneous turbulence and approximately constant in the wind tunnel, see [10]. An application of Girsanov's Theorem allows us to eliminate the $(-u \cdot \nabla u - U \cdot \nabla u) dt$ term at the cost of adding an exponential martingale,

$$M_t = \exp(-\int (U + u(B_s, s)) \cdot dB_s - \frac{1}{2} \int_0^t |U + u(B_s, s)|^2 ds),$$

9

where $B_t \in \mathbb{R}^3$ is an auxiliary Brownian motion, to each term in the Navier Stokes equation:

$$du = [\nu\Delta u + \nabla(\Delta^{-1}[\text{Trace}(\nabla u)])]M_t dt$$
$$+ \sum_{k \neq 0} d_k |k|^{\frac{1}{3}} M_t dt e_k(x) + \sum_{k \neq 0} c_k^{\frac{1}{2}} M_t db_t^k e_k(x) \qquad (6)$$
$$+ u \sum_{k \neq 0} \int_{\mathbb{R}} h_k(t,z) \bar{N}^k M_t(dt,dz).$$

For the statement and proof of Girsanov's Theorem, see pages $149-151$ of [22]. The Feynman-Kac Formula allows us to eliminate the term

$$u \times \sum_{k \neq 0} \int_{\mathbb{R}} h_k(t,z) \bar{N}^k M_t(dt,dz)$$

at the cost of adding a log-Poisson process

$$e^{\int_s^t dq} = \frac{1}{3}(\sum_{k \neq 0}^m \{\int_0^t \int_{\mathbb{R}} \ln(1+h_k) \bar{N}^k(ds,dz) + \int_0^t \int_{\mathbb{R}} (\ln(1+h_k) - h_k) m_k(ds,dz)\})$$

to each term in the Navier-Stokes equation. For the statement and proof of Feynman-Kac Formula, see pages $128-129$ of [22]. Thus, the new Navier Stokes equation becomes

$$du = [\nu\Delta u + \nabla(\Delta^{-1}[\text{Trace}(\nabla u)])]e^{\int_s^t dq} M_t dt$$
$$+ \sum_{k \neq 0} d_k |k|^{\frac{1}{3}} e^{\int_s^t dq} M_t dt e_k(x) + \sum_{k \neq 0} c_k^{\frac{1}{2}} e^{\int_s^t dq} M_t db_t^k e_k(x) \qquad (7)$$

$$(8)$$

Finally, we use the definition of mild (or Martingale) solutions of nonlinear stochastic partial differential equations (SPDE) in infinite-dimensional space:

Definition 3.1 *Consider the initial value SPDE problem*

$$du = (Au + F(t,u))dt + G(t,u)dB_t, \ u(x,0) = u_0.$$

A stochastic process $u(\omega,x,t)$ is a mild solution of this SPDE initial value problem (IVP) if

$$P(\int_0^t |u|_2^2(s)dt < \infty), \qquad P \text{ a. s.}$$

10

and

$$u(t) = e^{At}u_0 + \int_0^t e^{A(t-s)}F(s,u(s))ds + \int_0^t e^{A(t-s)}G(s,u(s))dB_s, \qquad P \text{ a. s.,}$$

where P is the probability measure in the associated probability space $(\Omega, \mathcal{F}, P)$.

For more information, see page 182 in [13]. One can then state a theorem for the existence of unique mild local (in time) solutions, see page 186 in [13]. Now, this theorem does not apply directly here, as the multiplicative noise concerns jumps and not only Brownian motion. However, a slight alteration of the proof gives local existence of solutions. The mild solution of the stochastic Navier Stokes equation, governing fully developed turbulence, is given by

$$u = e^{K(t)}e^{\int_0^t dq}M_t u^0 + \sum_{k \neq 0} c_k^{\frac{1}{2}} \int_0^t e^{K(t-s)}e^{\int_s^t dq}M_{t-s}db_s^k e_k(x) \qquad (9)$$

$$+ \sum_{k \neq 0} d_k \int_0^t e^{K(t-s)}e^{\int_s^t dq}M_{t-s}|k|^{\frac{1}{3}}dt e_k(x),$$

where K is the operator

$$K = \nu\Delta + \nabla\Delta^{-1}\text{Trace}(\nabla u\nabla), \qquad (10)$$

M_t is the above exponential martingale, $e_k(x) = e^{2\pi ikx}$ is a Fourier component complete with its own Brownian motion b_t^k, and the coefficients $c_k^{\frac{1}{2}}$ and d_k decay fast enough so that the series converges, see [7], Chapter 1. This is also the integral form of the stochastic Navier-Stokes equation (7).

   The integral equation (9) is equivalent to the stochastic Navier-Stokes initial value problem (7) for the small scales. It will be our main tool in computing the structure functions.

4   The Computation of the Structure Functions

In this section, we describe the calculation of the structure functions of turbulence, which will be compared with the experimental data. Using the stochastic Navier-

11

Stokes integral equation (9) from previous section, we have that

$$u(x,t) - u(y,t) = \tag{11}$$

$$\sum_{k \neq 0} \left[(c_k^{\frac{1}{2}} \int_0^t e^{K(t-s)} e^{\int_s^t dq} M_{t-s} db_s^k \tag{12}\right.$$

$$\left. + d_k \int_0^t e^{K(t-s)} e^{\int_s^t dq} M_{t-s} |k|^{\frac{1}{3}} ds)(e_k(x) - e_k(y)) \right],$$

where $u(x,t)$ and $u(y,t)$ are the flow velocities at two points x and y in the wind tunnel. This permits us to describe the computation of the structure functions:

$$S_p(x - y, t) = E(|u(x,t) - u(y,t)|^p).$$

First, we note that the expectation is actually a composition of three expectations, one for the Brownian motions in the Fourier series representation of the noise, denoted E_b, another for the log-Poisson process, denoted E_p, and the third E_B for the auxiliary Brownian motion in the Martingale in the last section. The log-Poisson expectation acts upon the term

$$e^{\int_s^t dq} = \exp\{\frac{\frac{2}{3}\ln|k| + N_k \ln(\frac{2}{3})}{3}\} = (|k|^{\frac{2}{3}}(\frac{2}{3})^{N_t^k})^{\frac{1}{3}},$$

given by the Feynman-Kac formula, see [7]. Then, we get that

$$E_p([|k|^{\frac{2}{3}}(\frac{2}{3})^{N_t^k}]^{\frac{p}{3}}) = |k|^{-(-\frac{2p}{9} + 2(1 - (\frac{2}{3})^{\frac{p}{3}}))},$$

see [7]. Notice the exponent above is the She-Leveque intermittency correction (1), denoted τ_p. Applying E_p also eliminates all terms $(e_k(x) - e_k(y))(e_j(x) - e_j(y))$ for $k \neq j$. Standard algebra and trigonometry gives

$$e_k(x) - e_k(y) = 2e^{\pi i k(x+y)} \sin(\pi k \cdot (x - y)).$$

12

Thus, we get that

$$E(|u(x,t) - u(y,t)|^p) = \tag{13}$$

$$E(|\sum_{k \neq 0} \left[(c_k^{\frac{1}{2}} \int_0^t e^{K(t-s)} e^{\int_s^t dq} M_{t-s} db_s^k \tag{14}$$

$$+ d_k \int_0^t e^{K(t-s)} e^{\int_s^t dq} M_{t-s} |k|^{\frac{1}{3}} ds)(e_k(x) - e_k(y)) \right] |^p)$$

$$= E_b(|\sum_{k \neq 0} \left[(c_k^{\frac{1}{2}} \int_0^t e^{K(t-s)} |k|^{-\tau_p} E_B(M_{t-s}) db_s^k) \tag{15}$$

$$+ d_k \int_0^t e^{K(t-s)} |k|^{-\tau_p} E_B(M_{t-s}) |k|^{\frac{1}{3}} ds \right] \times 2 e^{\pi k i (x+y)} \sin(\pi k \cdot (x-y)) |^p).$$

Now, we use the estimate for the action of the operator K on the Fourier components, replacing it with $\lambda_k = C|k|^{\frac{2}{3}} + 4\nu\pi^2|k|^2$, see [7]. A lower estimate is $-C|k|^{\frac{2}{3}} + 4\nu\pi^2|k|^2$. These estimates assume that the expectation of the norm of u in the Sobolev space $H^{\frac{11}{6}^+}$ is finite, see Lemma 2.7 in [7]. We will discuss this in more detail in a future paper. M_t is the exponential martingale:

$$M_t = \text{Exp}[\int (U+u) \cdot dB_s - \int \frac{|U+u|^2}{2} ds],$$

where $B_t \in \mathbb{R}^3$ is an auxiliary Brownian motion and $U+u$ is the Reynolds decomposition of the flow. A simple application of Ito's formula yields

$$M_t^p = 1 + \int_0^t (U+u) M_s \cdot dB_s + \frac{p(p-1)}{2} \int_0^t |U+u|^2 M_s^p ds.$$

Thus, we have

$$E_B[M_t^p] = 1 + \frac{p(p-1)}{2} \int_0^t E_B[|U+u|^2 M_s^p] ds$$

$$\leq 1 + \frac{p(p-1)}{2} \int_0^t \sup_x |U+u|^2 E_B[M_s^p] ds.$$

Thus by Grönwall's inequality

$$E_B[M_t^p] \leq e^{\frac{p(p-1)}{4} \int_0^t \sup_x (|U|^2 + |u|^2) dt}.$$

13

The sup in x frees the expectation from the expectation of the auxiliary Brownian motion, used to define the Martingale, and the exponent of the right hand side is easily estimated by the same methods as below

$$E_b[\sup_x(|U|^2 + |u|^2)] \leq \sup_x |U|^2 + \frac{1}{C^2}\sum_{k\neq 0}\frac{(C/2)c_k + d_k^2}{|k|^{\zeta_2}} = \text{Constant.}$$

This implies that $E_B[M_t^p]$ only adds a constant, first to the exponents and then to the denominators, in the structure functions below and we will ignore it.

Finally, we take the absolute value and expand the polynomial expression in (13). To ultimately compute the structure functions, we use Ito's Lemma

$$E[(\int_S^T f(t,w)dB_t)^2] = \int_S^T E[(f(t,w))^2]dt$$

to turn any even power of the stochastic integral into a deterministic integral, which can then be solved for using standard calculus. For odd powers, we use the fact that

$$E[\int_S^T f dB_t] = 0$$

to eliminate such terms. We then find the first-order structure function is given by

$$E(|u(x,t) - u(y,t)|) = S_1(x,y,t)$$
$$= \frac{2}{C}\sum_{k\in\mathbb{Z}^3\setminus\{0\}}\frac{|d_k|(1 - e^{-\lambda_k t})}{|k|^{\zeta_1} + \frac{4\pi^2\nu}{C}|k|^{\zeta_1 + \frac{4}{3}}}|\sin(\pi k\cdot(x-y))|, \quad (16)$$

where $|\cdot|$ denotes the vector norm in $\mathbb{R}^3$. The second-order structure function is given by

$$E(|u(x,t) - u(y,t)|^2) = S_2(x,y,t)$$
$$= \frac{4}{C^2}\sum_{k\in\mathbb{Z}^3}\left[(|\sin^2(\pi k\cdot(x-y))|)\right.$$
$$\left\{\frac{\frac{C}{2}c_k(1 - e^{-2\lambda_k t})}{|k|^{\zeta_2} + \frac{4\pi^2\nu}{C}|k|^{\zeta_2 + \frac{4}{3}}}\right. \quad (17)$$
$$\left.\left.+ \frac{|d_k|^2(1 - e^{-\lambda_k t})}{|k|^{\zeta_2} + \frac{8\pi^2\nu}{C}|k|^{\zeta_2 + \frac{4}{3}} + \frac{16\pi^4\nu^2}{C^2}|k|^{\zeta_2 + \frac{8}{3}}}\right\}\right]$$

14

where $c_k = |c_k^{\frac{1}{2}}|^2$. The third-order structure function is given by

$$
\begin{aligned}
E(|u(x,t) - u(y,t)|^3) &= S_3(x,y,t) \\
&= \frac{8}{C^3} \sum_{k \in \mathbb{Z}^3} \Big[(|\sin^3(\pi k \cdot (x-y))|) \\
&\quad \Big\{ \frac{\frac{C}{2} c_k |d_k| (1 - e^{-2\lambda_k t})(1 - e^{-\lambda_k t})}{|k|^{\zeta_3} + \frac{8\pi^2 \nu}{C} |k|^{\zeta_3 + \frac{4}{3}} + \frac{16\pi^4 \nu^2}{C^2} |k|^{\zeta_3 + \frac{8}{3}}} \\
&\quad + \frac{|d_k|^3 (1 - e^{-\lambda_k t})^3}{|k|^{\zeta_3} + \frac{12\pi^2 \nu}{C} |k|^{\zeta_3 + \frac{4}{3}} + \frac{48\pi^4 \nu^2}{C^2} |k|^{\zeta_3 + \frac{8}{3}} + \frac{64\pi^6 \nu^3}{C^3} |k|^{\zeta_3 + 4}} \Big\} \Big]
\end{aligned}
\tag{18}
$$

The general p-th order structure function is given by

$$
S_p(x,y,t) = \frac{2^p}{C^p} \sum_{k \neq 0} A_p \times |\sin^p[\pi k \cdot (x-y)]|,
\tag{19}
$$

where

$$
A_p = \frac{2^{\frac{p}{2}} \Gamma(\frac{p+1}{2}) \sigma_k^p {}_1F_1(-\frac{1}{2}p, \frac{1}{2}, -\frac{1}{2}(\frac{M_k}{\sigma_k})^2)}{|k|^{\zeta_p} + \frac{p_k \pi^2 \nu}{C} |k|^{\zeta_p + \frac{4}{3}} + O(\nu^2)},
\tag{20}
$$

where Γ is the gamma function, ${}_1F_1$ is the hypergeometric function, $M_k = |d_k|(1 - e^{-\lambda_k t})$, $\sigma_k = \sqrt{(\frac{C}{2} c_k (1 - e^{-2\lambda_k t}))}$, and p_k is different for each denominator term in the series. Note that the Reynolds number dependence is captured via the viscosity term ν. C is a constant approximating the norm of the small-scale velocity of the flow. It will allowed to vary across structure functions to accommodate a relative change in the mean and the large deviations.

The equalities for the structure function above are really lower estimates because the action of e^{Kt} on the kth Fourier component is estimated by $e^{-\lambda_k t}$, where λ_k is an overestimate. We also get an overestimate of the structure functions by using the lower estimate $-C|k|^{\frac{2}{3}} + 4\nu\pi^2|k|^2$ instead of λ_k. However, since the Kolmogorov-Obuhov cascade is a forward cascade in three dimensions, that is the energy flows from high to low wavenumbers, the lower estimate of the structure functions is sharp and we drop the inequality in favor of the equality. The other thing to notice is that we are not using the eigenfunctions of the operator K and the λ_ks are not the eigenvalues of K. It turns out to be much simpler to work with the Fourier components instead of the eigenfunctions of K.

The above formulas clearly distinguish the stochastic closure theory (SCT) from previous theories on turbulence. SCT shows that the correct basis for the pth structure function, in Fourier space, is the collection of sine components of the lag variable, indexed by different wavenumbers and raised to the power p. The coefficients for this basis are given by the formula (20). This allows us to represent all structure functions as functions of the lag variable for all Reynolds numbers and all power p. Such a result has been unattainable until now. It permits a complete characterization of the experimental data for the structure functions in homogeneous turbulence.

4.1 The One-dimensional Structure Functions

We want to fit the structure functions (19) to the experimental data collected in the VDTT. To do this we have to reduce the three-dimensional structure functions to one-dimensional ones. We will perform the reduction in this subsection.

We consider structure functions where the measurements are taken at two distinct points along the length of the tunnel, in the direction of the mean velocity. These are called the longitudinal structure functions, $S_p(r,t)$, where $r = x - y$, is a vector along the main axis of the tunnel. One can also consider the transversal structure functions, $S_p(q,t)$, where $q = x - y$, is a vector in the radial direction of the tunnel, perpendicular to r. In homogeneous turbulence these two structure functions are not independent. Their correlation matrix is given by [23]:

$$D_{ij} = E[(u_i(x,t) - u_i(y,t))(u_j(x,t) - u_j(y,t))] = S_2(r,t)I + (S_2(r,t) - S_2(q,t))\frac{r_i r_j}{r^2},$$

where I is the identity matrix in $\mathbb{R}^3 \times \mathbb{R}^3$, and

$$S_2(q,t) = S_2(r,t) + r\frac{\partial}{\partial r}S_2(r,t),$$

with $r = |r|$, $|\cdot|$ denoting the vector norm in $\mathbb{R}^3$. For $\eta << r$, D_{ij} is expected to reduce to

$$D_{ij} = C_2(\varepsilon r)^{2/3}(\frac{4}{3}I - \frac{1}{3}\frac{r_i r_j}{r^2}).$$

Thus in $\mathbb{R}^3$ the correlation matrix is determined by longitudinal structure function $S_2(r,t)$ alone and we will restrict our attention to the longitudinal structure functions.

Consider the longitudinal third-order structure function given by the SCT,

$$S_3(r,t) = \frac{8}{C^3} \sum_{k \in \mathbb{Z}^3} \left[(|\sin^3(\pi k \cdot r)|) \left\{ \frac{\frac{C}{2} c_k |d_k| (1 - e^{-2\lambda_k t})(1 - e^{-\lambda_k t})}{|k|^{\zeta_3} + \frac{8\pi^2 v}{C} |k|^{\zeta_3 + \frac{4}{3}} + \frac{16\pi^4 v^2}{C^2} |k|^{\zeta_3 + \frac{8}{3}}} \right. \right.$$
$$\left. \left. + \frac{|d_k|^3 (1 - e^{-\lambda_k t})^3}{|k|^{\zeta_3} + \frac{12\pi^2 v}{C} |k|^{\zeta_3 + \frac{4}{3}} + \frac{48\pi^4 v^2}{C^2} |k|^{\zeta_3 + \frac{8}{3}} + \frac{64\pi^6 v^3}{C^3} |k|^{\zeta_3 + 4}} \right\} \right],$$

where $c_k = c_1 + c_2 + c_2$, $|d_k| = \sqrt{d_1^2 + d_2^2 + d_2^2}$ and $|k| = \sqrt{k_1^2 + k_2^2 + k_2^2}$, and $r = x - y$. If we take $r = (r,0,0)$ to lie along the axis of the VDTT (cylinder), then $r \cdot k = (rk_1,0,0)$ and if we ignore k_2 and k_3 in the denominator of S_2, and take $t \to \infty$, we get the inequality

$$S_3(r,t) \leq \frac{8}{C^3} \sum_{k_1 \neq 0} \left[(|\sin^3(\pi k_1 r)|) \left\{ \frac{\frac{C}{2} \tilde{c}_{k_1} |\tilde{d}_{k_1}|}{|k_1|^{\zeta_3} + \frac{8\pi^2 v}{C} |k_1|^{\zeta_3 + \frac{4}{3}} + \frac{16\pi^4 v^2}{C^2} |k_1|^{\zeta_3 + \frac{8}{3}}} \right. \right.$$
$$\left. \left. + \frac{|\tilde{d}_{k_1}|^3}{|k_1|^{\zeta_3} + \frac{12\pi^2 v}{C} |k_1|^{\zeta_3 + \frac{4}{3}} + \frac{48\pi^4 v^2}{C^2} |k_1|^{\zeta_3 + \frac{8}{3}} + \frac{64\pi^6 v^3}{C^3} |k_1|^{\zeta_3 + 4}} \right\} \right],$$

because $\zeta_3 = 1$, where $\tilde{c}_{k_1} = \sum_{k_2 \neq 0} \sum_{k_3 \neq 0} c_{(k_1,k_2,k_3)}$, $|\tilde{d}_{k_1}| = \sum_{k_2 \neq 0} \sum_{k_3 \neq 0} |d_{(k_1,k_2,k_3)}|$. We have used the convexity of the functions $f(x) = x^p$, $p \geq 1$ to take the sum into the powers, here $p = 1, 3$. This upper estimate, that is supposed to be close, reduces the three dimensional S_3 to the one dimensional one. The argument for all the structure functions S_p, $p \geq 3$, is similar but the argument does not hold for $p = 1$, or 2, because $\zeta_1 = 0.37$ and $\zeta_2 = 0.696$ in the She-Leveque model, so both are less than one. This means that the upper estimate does not hold for all $|k|$s, only the ones that are big enough so that the second term in the denominators of S_1 and S_2 dominates the first. We will use the upper estimate with this understanding. We will compare the one-dimensional structure function with experimental data and drop the subscript 1 on k_1. Thus the general p-th one-dimensional longitudinal structure function, in the stationary state, is given by

$$S_p(r, \infty) \leq \frac{2^p}{C^p} \sum_{k \neq 0} \frac{2^{\frac{p}{2}} \Gamma(\frac{p+1}{2}) \sigma_k^p {}_1 F_1(-\frac{1}{2} p, \frac{1}{2}, -\frac{1}{2}(\frac{M_k}{\sigma_k})^2)}{|k|^{\zeta_p} + \frac{p_k \pi^2 v}{C} |k|^{\zeta_p + \frac{4}{3}} + O(v^2)} |\sin^p[\pi k r]|, \qquad (21)$$

where Γ is the gamma function, ${}_1 F_1$ is the hypergeometric function, $M_k = |\tilde{d}_k|$, $\sigma_k^2 = \frac{C}{2} \tilde{c}_k$, and p_k is different for each denominator term in the series. Note that the Taylor-Reynolds number dependence is captured via the viscosity term v, as

17

the Taylor Reynolds number is given by $U\lambda/\nu$. C is a constant approximating the mean velocity fluctuation of the flow. The upper estimate is understood to hold for $p = 1, 2$, when $|k|$ is large enough.

We can think about the triple sum as an integral

$$\sum_{k \in \mathbb{Z}^3 \setminus \{0\}} c_k \sim \int_0^\infty \int_\omega c_k d\omega |k|^2 d|k| = \int_0^\infty \tilde{c}_k dk \sim \sum_{k \neq 0} \tilde{c}_k,$$

where $|k|$ is the radius of the three-vector k, and $d\omega$ is the angular part of the volume element. This means that

$$\tilde{c}_k = \int_\omega c_k d\omega |k|^2,$$

is the integral of c_k over a sphere of radius k is Fourier space, analogous to the energy shell in the Kolmogorov-Obukhov cascade. Thus, whereas $c_k \sim \frac{1}{k^{3+\varepsilon}}$, where $k = |k|$, in order for the sum to converge, $\tilde{c}_k \sim \frac{1}{k^{1+\varepsilon}}$. A similar argument applies to $\sum_{k \in \mathbb{Z}^3 \setminus \{0\}} |d_k|$ For this reason we expect the exponent m of k below to satisfy $m > 1$. We will in fact make the ansatz,

$$\tilde{c}_k = \sqrt{\frac{2}{\pi}} \frac{b}{b^2 + k^m}, \quad \tilde{d}_k = \sqrt{\frac{2}{\pi}} \frac{a}{a^2 + k^m}, \tag{22}$$

where $\tilde{c}_k$ and $\tilde{d}_k$ are the one-dimensional versions of the coefficients in the structure functions, to approximate the experimental data. Provided that m is greater than 1, the series determining the one dimensional restriction of the structure functions (21) will converge. The thinking here is that there is a universal coefficient m for each Reynolds number that will determine how fast the sine series converges, and thus the spatial smoothness of the structure functions. Thus for k large, $\tilde{c}_k$ and $\tilde{d}_k \sim \frac{1}{k^m}$. Moreover, we are (optimistically) assuming that the two contributions $\tilde{c}_k$ and $\tilde{d}_k$, to the large eddies, also scale with the order of the structure functions and can be characterized by a number b, respectively a, for each Taylor-Reynolds number. Thus for k small, $\tilde{c}_k \sim \frac{1}{b}$ and $\tilde{d}_k \sim \frac{1}{a}$. This turns out to work reasonably well, see Table 5.

In summary, we reduce the coefficients for the three-dimensional structure functions, c_k and d_k, to the ones for the one-dimensional structure functions, $\tilde{c}_k$ and $\tilde{d}_k$. We then fit the formulas for the one-dimensional structure functions to the data, and propose a simple ansatz (22), for the coefficients' dependence on the Taylor-Reynolds number and the wavenumber $1/k$.

18

5 Comparison of the Model with the Data

The VDTT is capable of using pressurized inert gases as working fluids. Specifically, the use of pressurized Sulfur Hexafluoride with a low kinematic viscosity enables classical grid experiments at R_λ up to 1600. The turbulence in the VDTT was generated by a fixed grid of crossed bars, and is called classical grid turbulence [12, 11]. The classical grid disturbed the free flow mechanically at the upstream end of the test section. In the wake of the grid, the turbulence evolved along the length of the tunnel without the middle region being substantially influenced by the walls of the tunnel [10]. The measurements were made with a Dantec StreamLine hot-wire anemometry system, using NSTAPs developed at Princeton University, see [31]. The hot-wire probes were at a distance of 7.1 meters downstream from the 186.6 mm classical grid, so that the turbulence evolved through at least one eddy turnover time. Taylor's frozen flow hypothesis is used to extract x and r from the time series of the probe as in [10]. Measurements were taken for Taylor Reynolds Numbers 110, 264, 508, 1000, and 1450. The pertinent parameters for the data are given Table 1. For more information about the experiments, see [29, 28]. Each measurement was taken over five minutes and sampled at 60kHz, giving $1.8(10^7)$ data points.

The longitudinal velocity differences are

$$\delta u(r,t) = u(y,t) - u(x,t) = u(x+r,t) - u(x,t)$$

where u, x and r are parallel vectors along the x-axis. The system length in the tunnel is an important value when fitting the data since we scale the lag variable, r, $\frac{r/\eta}{\text{system length}} = (x-y)$, with the system length. The system length in our case is the mesh size of the grid, and not the square root of the cross sectional area of the tunnel, for instance. The structure functions were plotted against r/η, where r is the distance between positions x and y as given by the Taylor Frozen Flow Hypothesis and η is the Kolmogorov length scale. In order for our sine series formula to capture the entire data set, we divided r/η by its maximum value for which we computed structure functions, which was $\frac{r}{\eta} = 19540$. We also introduced a variable, D, so that we substituted

$$\frac{r}{\eta}/(19540(D))$$

for $x-y$ in the formulas. The fitted values for D are given in Table 5. Note that D is one of the four parameters which are not active over the range of Taylor-Reynolds numbers, which is shown in Figure 7 and will be justified later.

Taylor Reynolds Number	η	L	ν
110	1025	165.1	$1.55(10^{-5})$
264	162	102.5	$2.34(10^{-6})$
508	91	123.9	$1.00(10^{-6})$
1000	36	136.6	$2.91(10^{-7})$
1450	22	129.5	$1.50(10^{-7})$

Table 1: Here, η is the Kolmogorov length scale given in micrometers, L is the integral length scale given in millimeters, and ν is the viscosity given in m^2/s. The data here is at the furthest measured point downstream of the grid, as η and L evolve downstream.

Fitting was done in Mathematica using the built-in "findfit" function. To bound computational time reasonably, the series given in Section 2 were limited to one thousand terms. Because initial fitting to the formulas given in Section 2 proved not to be effective, we permitted the first two sine terms in the expansion to have free coefficients to allow for variation in the nonuniversal largest scales of the flow [9]. In other words, the new model used to fit the data is given by

$$S_p = A_1 |\sin[(\pi \times r)/(19540.3(D))]| + A_2 |\sin^2[(2\pi \times r)/(19540.3(D))]| \quad (23)$$

$$+ \sum_{k=3} \frac{2^p}{C^p} A_p |\sin^p[\pi k \cdot (x-y)]|, \quad (24)$$

where A_p is given by (20). This was done for all structure function fits.

As it stands right now, that leaves us with seven parameters for the fits, namely a, b, m, C, D, A_1, and A_2. However, only three parameters are active over the entire inertial range, specifically a, b, and m, in the sense that they are changing the relative weights of the Fourier components of the solution $u(x,t)$. The parameter D measures the system length correction for large Reynolds numbers. This correction serves to place the transition from the dissipative range to the inertial range. The parameter C measures the root-mean squared velocity whereas A_1 and A_2 measure the influence of the large eddies upon the grid. These three parameters measure the transition out of the inertial range. This is shown in Figures 7, 16, and 17, and will be justified later. Through experimentation, we found the best result when using the fourth-order structure functions for each Taylor Reynolds Number to fix the coefficients a, b, and D.

Tables 2, 3, and 4 contain the fitted values of A_1, A_2 and C respectively, as

20

Re Lambda	110	264	508	1000	1450
Second-Order	0.00744	.0153	.0169	.0183	.0195
Third-Order	.00154	.00162	.00484	.00564	.00664
Fourth-Order	.000384	.00189	.00228	.00251	.00305
Sixth-Order	.0000341	.000431	.000566	.000552	.000691
Eighth-Order	$3.12(10^{-6})$	.0000839	.000122	.000144	.000204

Table 2: The fitted values for A_1 in eq. (23)

Re Lambda	110	264	508	1000	1450
Second-Order	.00285	.00583	.00653	.00697	.00666
Third-Order	.000872	.00124	.00526	.00488	.00395
Fourth-Order	.000174	.000746	.000804	.001	.0006
Sixth-Order	$4.24(10^{-6})$	-.0000756	-.00011	.0000919	.0000654
Eighth-Order	$1.04(10^{-6})$	.0000127	.0000147	.0000264	$-4.71(10^{-7})$

Table 3: The fitted values for A_2 in eq. (23)

(a)

(b)
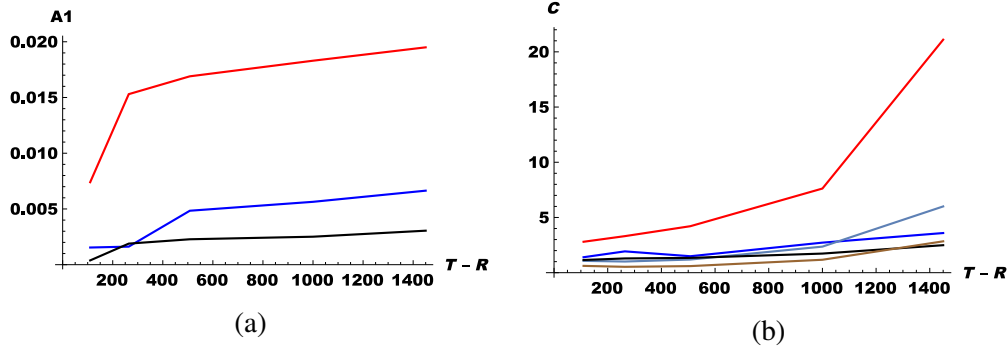
Figure 1: (a) The values of the coefficient A_1 of the first Fourier component, as a function of the Taylor-Reynolds number, from Table 2. Top (red) 2nd moment, second from top (blue) 3rd moment, third from top (black) 4th moments. The higher moments give negligible correction, whereas the first three change little, notice the scale, over the range of T-R numbers in the experiment.
(b) The values of the coefficient C, as a function of the Taylor-Reynolds number, from Table 4, top (red) 2nd moment (root means square size), lower, the higher moments. Notice that neither (a) or (b) are plotted on a log scale.

Taylor Reynolds Number	110	264	508	1000	1450
Second-Order	2.8	3.31	4.21	7.62	21.1
Third-Order	1.4	1.93	1.49	2.72	3.59
Fourth-Order	1.07	1.01	1.19	2.36	6
Sixth-Order	1.15	1.29	1.34	1.73	2.49
Eighth-Order	0.616	.531	.596	1.17	2.84

Table 4: The fitted values for C in eq. (23)

Taylor Reynolds Number	a	b	D
110	11.64	0.01612	1.569
264	9.581	0.05236	1.769
508	8.314	0.06504	1.518
1000	3.792	0.09247	1.32
1450	2.684	0.4092	1.3

Table 5: The fitted values for a, b, and D in eq. (23). Note that these parameters are grouped as they are independent of the order of the structure functions.

Taylor Reynolds Number	110	264	508	1000	1450
Second-Order	1.563	1.16	1.069	.8965	.9148
Third-Order	1.408	1.185	0.922	.6488	.5262
Fourth-Order	1.269	.8751	.7936	.5554	.4865
Sixth-Order	.98607	.5055	.5192	.4339	.3398
Eighth-Order	.9711	.5924	.5755	.3771	.2482

Table 6: The fitted values for m in eq. 23

described in (23). Note that A_1, A_2, C, and m are given their own tables as they change with the order of the structure function, whereas a, b, and D are placed in the same table as they do not. Consider Figure 1a that shows the values of the coefficient A_1 as a function of the Taylor-Reynolds number taken from Table 2. We show that the values are small and do not change much over the range of T-R numbers in the experiment. The figure shows the values based on the first three structure functions do not change much of the whole over the range of T-R numbers in the experiment and the higher order structure functions give negligible correction. One can think of the second-order structure function as the root-mean square size and the higher order ones measure the roughness. Table 3 shows that the same analysis applies to the coefficient A_2 except that its values are even smaller. Consequently we omit the plot of A_2. Table 4 shows that the parameter C increases over the range of T-R numbers in the experiment and Figure 1b shows its plot corresponding to the increasing structure functions. We see that only the 2nd moment (red), measuring the root-mean square size of the mean fluctuation velocity, increases significantly over the range of T-R numbers in the experiment. The plots corresponding to the higher moments increase significantly less, although they indicate that the mean velocity is getting spatially rougher. However, this is not influencing much the balance of the Fourier components in the Fourier representation of $u(x,t)$ compared to the significant changes in the parameters a, b and m discussed below. It simply measures the increase of the mean turbulent velocity as the turbulence increases. Table 5 shows the parameter D does not change with the order of the structure functions and does not change much over the range of T-R numbers in the experiment.

6   Evaluation of the Model

In this section we present the results of the fits to the data. In the figures 2, 3, 4, 5, and 6, the blue diamonds are the data from the experiment while the red lines are the SCT theory predictions. All the plots are on a log-log scale except for a single plot of the second-order structure function at Taylor Reynolds Number 110, this latter plot is included for perspective. The agreement between the theory is satisfactory for most orders of the structure functions and for most Reynolds numbers. For the highest Reynolds numbers and highest order (sixth- and eighth-order) structure functions, we see differences between the theory and experiment at the smallest scales. In general, we note that the fits become less accurate as we increase the order of the structure functions. The fits for the second-, third-, and

23

fourth-order structure functions are generally better than the fits for the sixth- and eighth-order structure function fits, which are rougher. This is expected from the theory given by in [7], and will be explored further in a future paper.

Table 5 gives the fitted values for a and b that change significantly over the range of T-R numbers in the experiment, see Figure 8. This table shows that the Central Limit Theorem term,

$$\bar{D} = \sum_{k \neq 0} c_k^{\frac{1}{2}} db_t^k e_k(x), \ c_k^{\frac{1}{2}} = \sqrt{\frac{2}{\pi}} \frac{b}{b^2 + k^m},$$

as given by b has a greater influence for smaller Taylor Reynolds numbers than the Large Deviation Principle term:

$$D' = \sum_{k \neq 0} d_k \eta_k dt e_k(x), \ d_k = \sqrt{\frac{2}{\pi}} \frac{a}{a^2 + k^m},$$

given by a, as for small values of k, these terms essentially become $\frac{1}{a^2}$ and b, respectively, because b is small. As the Reynolds number goes up, we do see an increasing influence of b dominating the increase of $\frac{1}{a^2}$, see the plot in Figure 8 (b). Thus the contribution of the Central Limit Theorem is greater.

The values of the exponent m of the wavenumber $k = k_1$ are given in Table 6. Their change over the inertial range seems small, but since m is and exponent the influence on the weight of the Fourier components of $u(x, t)$ is highly significant. In general the exponents are larger or very close to 1, at least near the top of the table. The first (top) line in Table 6, corresponding to the second-order structure function, verifies the hypothesis concerning the coefficients c_k and d_k in Sections 2 and 4. The energy shell coefficient $\tilde{c}_k$ and $\tilde{d}_k$ should decay as $|k|^{-m}$, $m > 1$. All the exponents in the first line in Table 6 satisfy this except the last two. However, both still lie within the fitting uncertainty and may be explained by the Reynolds number corrections absorbing the weight of the power. Thus the exponents $m(R_\lambda)$ in the first line depend on R_λ, but approach 1 as R_λ becomes large. We would expect the exponents to remain above one for the rest of the lines on the table, but this is not the case. We will seek to explain this result in a future paper.

7 The Improved SCT Model

The comparison of theory and data for homogeneous turbulence now produces a much improved Stochastic Closure Model, removing the infinitely many coefficients c_k, d_k, and h_k from Equation (7). What we find is that the large scales satisfy

equation (4), whereas the small scale flow satisfies the stochastic Navier-Stokes equation,

$$du + u \cdot \nabla u dt = (\nu \Delta u + \nabla(\Delta^{-1}[\text{Trace}(\nabla u)]))dt - u \cdot \nabla U - U \cdot \nabla u$$

$$+ \sum_{k \neq 0} \left(\frac{\mathbf{a}}{|a|^2 + |k|^m} \right) |k|^{-\frac{5}{3}} dt e_k(x) + \sum_{k \neq 0} \frac{\mathbf{b}^{1/2}}{(|b|^2 + |k|^m)^{1/2}} |k|^{-2} db_t^k e_k(x)$$

$$\tag{25}$$

$$- u \frac{1}{3} \sum_{k \neq 0} \bar{N}_t^k dt,$$

where $\mathbf{a}, \mathbf{b}^{1/2}, k \in \mathbb{R}^3$, $a = |\mathbf{a}|$, and $b = |\mathbf{b}|$. The improved SCT model depends on three parameters a, b and m, which are all function of the Taylor-Reynolds number R_λ. A plot of a and b from Table 5 are shown in Figure 8 (a). It shows that the Large Deviation coefficient a is larger than the Central Limit Theorem coefficient b. But this is deceiving since the right comparison is between $1/a^2$ and b for small wavenumber k, because of the form of the coefficients c_k, d_k in (22). This comparison is shown in Figure 8 (b). We see that b is larger than $1/a^2$ and dominates for large Reynolds numbers. For large wavenumbers k, b dominates even more because now it is compared with a^2/k^2. The conclusion is that the Central Limit Theorem term is the main contributor to the noise in the velocity differences, and the bias given by the Large Deviation term is only significant for small wavenumbers k and small Reynolds numbers.

The coefficient C that appears in the computation of the structure functions (21) is not constant for each Taylor-Reynolds number, see Table 4, because it measures both the size of the velocity fluctuations and the relative strength of the Center Limit Theorem term and the Large Deviation term in the noise. However, it does not vary much over the center part of Table 4 as a function of the Taylor-Reynolds number. The exponent m also varies with Taylor-Reynolds number. However, it also does not vary much with the Taylor-Reynolds number above the diagonal, as indicated by the bold numbers, in Table 6.

7.1 The Characterization of the Noise

We will now answer the question: "What is the noise in homogeneous turbulence?" based on the improvements of the SCT model. This is the question that was stated in Section 3 and partially answered by the original SCT model. We can completely answer the question and characterize the noise appearing in the
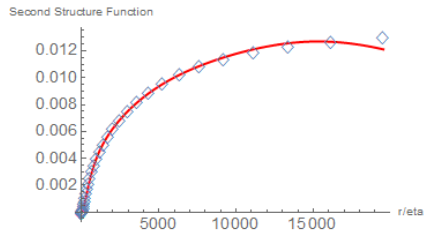
(a) Second-Order Structure Function, Normal Scale
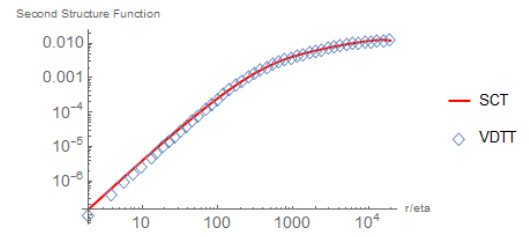
(b) Second-Order Structure Function
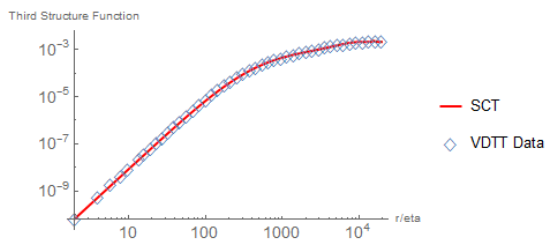
(c) Third-Order Structure Function
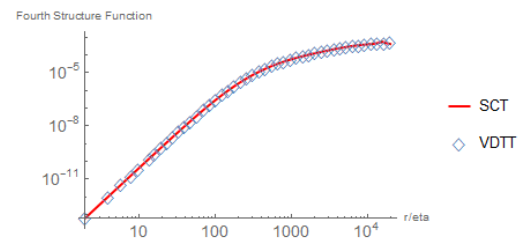
(d) Fourth-Order Structure Function
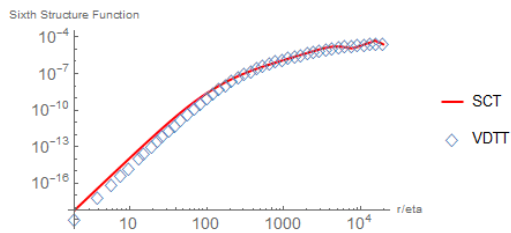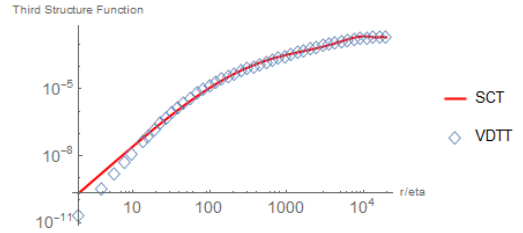
(e) Sixth-Order Structure Function
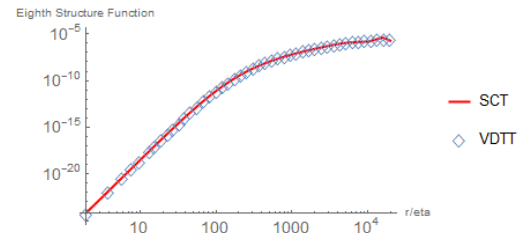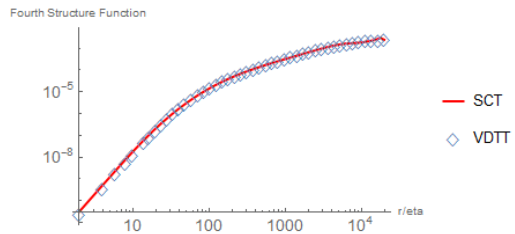
(f) Eighth-Order Structure Function

Figure 2: Taylor Reynolds Number 110. Note that the plots (b)-(f) are made on a log-log scale. The blue diamonds correspond to the data from the VDTT whereas the red line is the fitted SCT
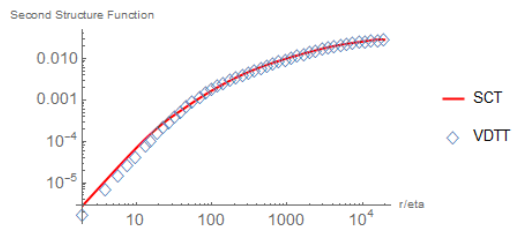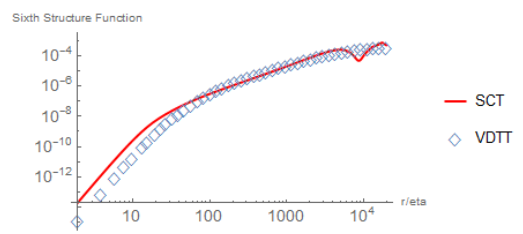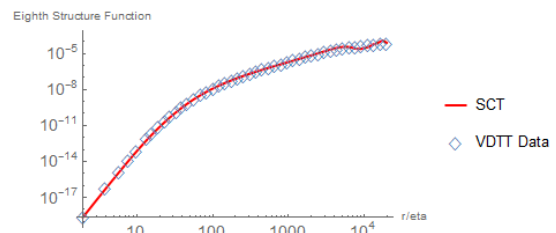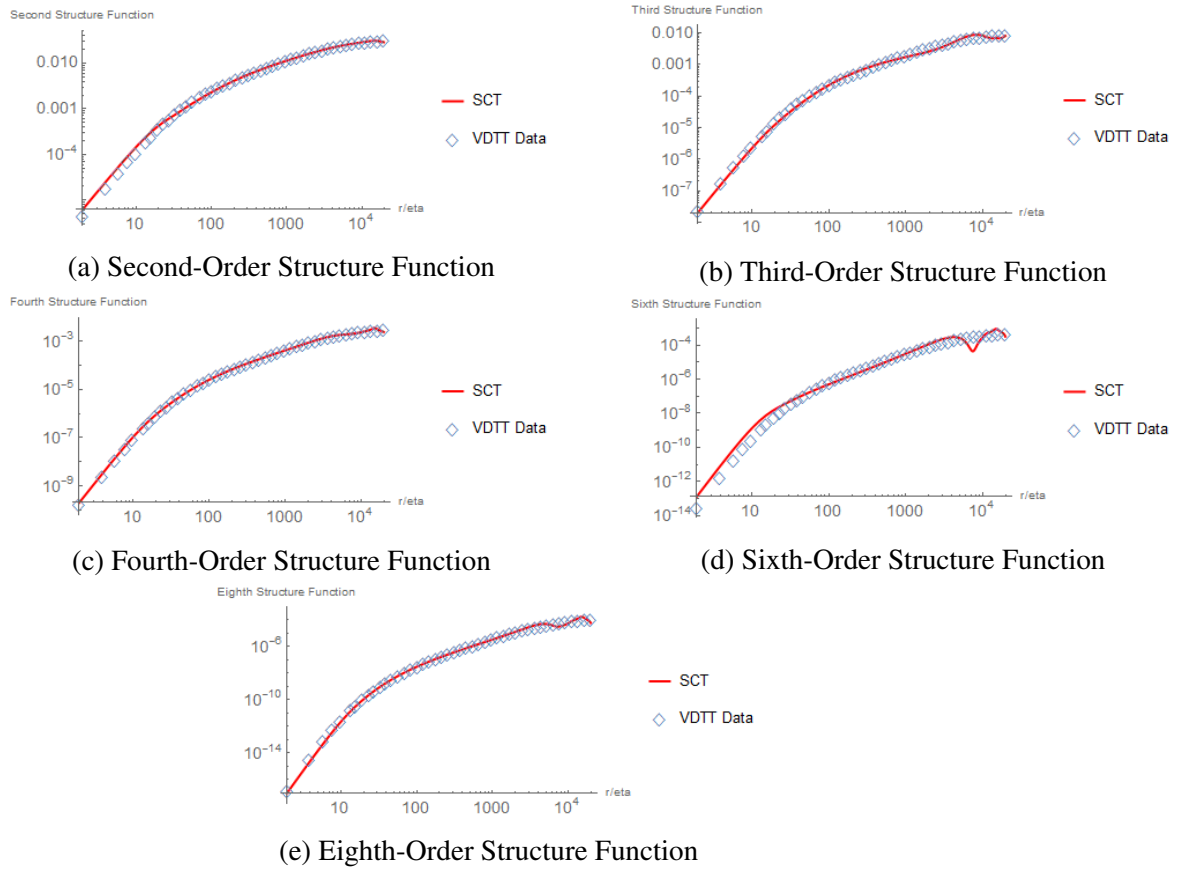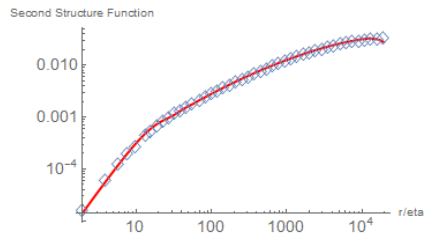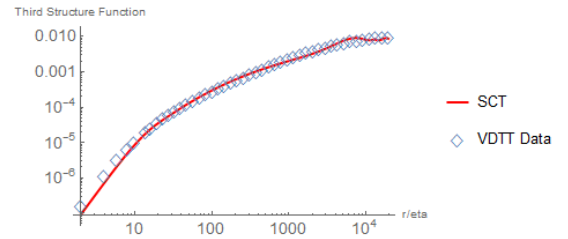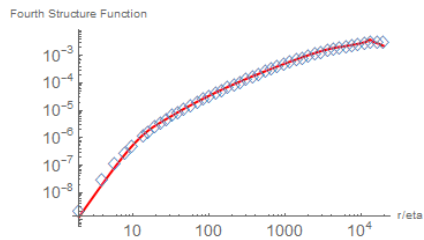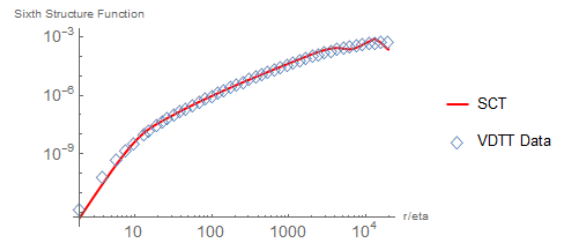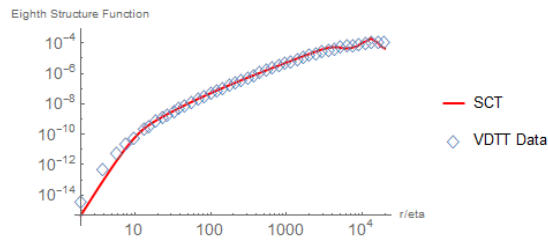
(a) Second-Order Structure Function

(b) Third-Order Structure Function

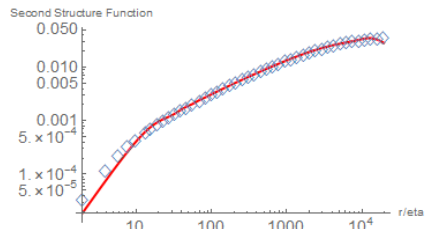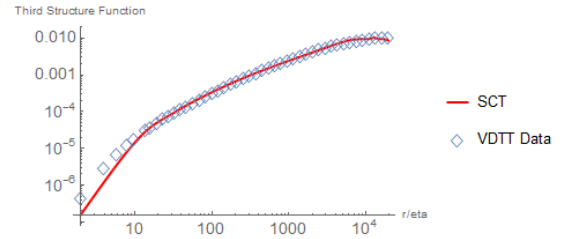(c) Fourth-Order Structure Function

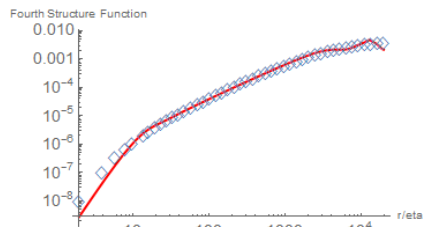(d) Sixth-Order Structure Function

(e) Eighth-Order Structure Function

Figure 3: Taylor Reynolds Number 264. Note that the plots are made on a log-log scale. The blue diamonds correspond to the data from the VDTT whereas the red line is the fitted SCT
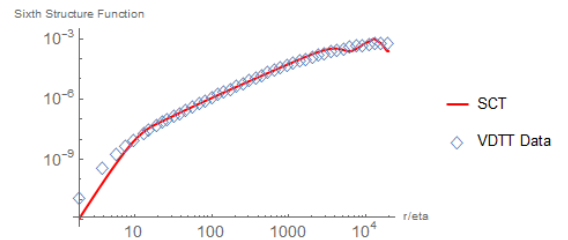
(a) Second-Order Structure Function

(b) Third-Order Structure Function

(c) Fourth-Order Structure Function

(d) Sixth-Order Structure Function

(e) Eighth-Order Structure Function

Figure 4: Taylor Reynolds Number 508. Note that the plots are made on a log-log scale. The blue diamonds correspond to the data from the VDTT whereas the red line is the fitted SCT
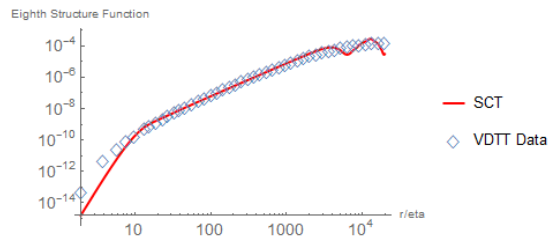
(a) Second-Order Structure Function

(b) Third-Order Structure Function

(c) Fourth-Order Structure Function

(d) Sixth-Order Structure Function

(e) Eighth-Order Structure Function

Figure 5: Taylor Reynolds Number 1000. Note that the plots are made on a log-log scale. The blue diamonds correspond to the data from the VDTT whereas the red line is the fitted SCT

(a) Second-Order Structure Function

(b) Third-Order Structure Function

(c) Fourth-Order Structure Function

(d) Sixth-Order Structure Function

(e) Eighth-Order Structure Function

Figure 6: Taylor Reynolds Number 1450. Note that the plots are made on a log-log scale. The blue diamonds correspond to the data from the VDTT whereas the red line is the fitted SCT

30

(a) Fourth Structure Function as shown in figure 5

(b) Fourth Structure Function at $D = 0.920864$
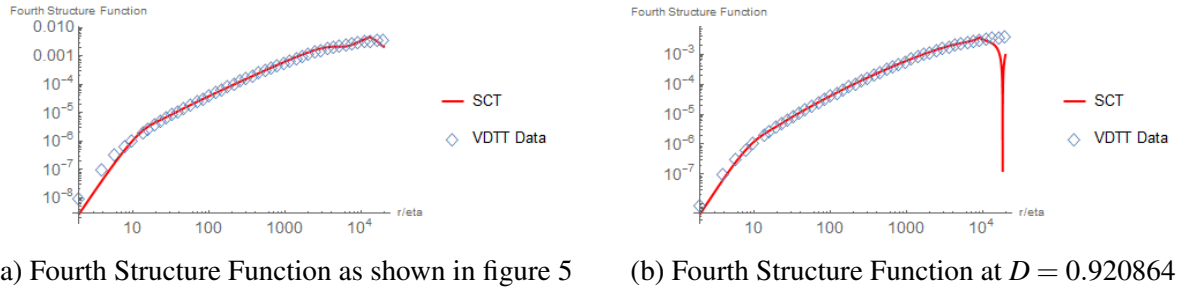
Figure 7: The two different fits for Taylor Reynolds number 1450. Note the downward peak resulting from the Sine series wanting to return to zero before the last data point.
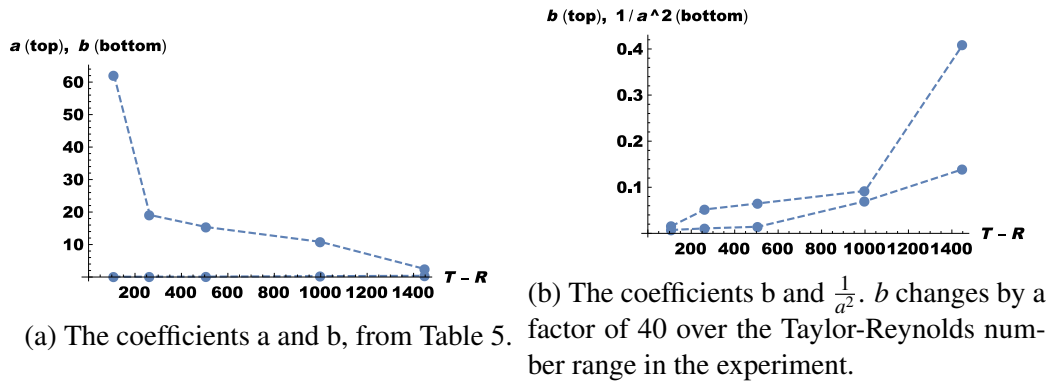

(a) The coefficients a and b, from Table 5.

(b) The coefficients b and $\frac{1}{a^2}$. b changes by a factor of 40 over the Taylor-Reynolds number range in the experiment.

Figure 8: The dependence of the coefficients, in the improved SCT model (25), on the Taylor-Reynolds number. The coefficient $\frac{1}{a^2}$ makes the large deviation contribution in (25) so it is plotted separately against b. Note that a versus b is included for completeness but due to the nature of the Fourier coefficients c_k and d_k as defined in (22), the ideal comparison is b against $\frac{1}{a^2}$.

(a) Second-order Structure Function

(b) Third-order Structure Function

(c) Fourth-order StructureFunction

(d) Sixth-order Structure Function

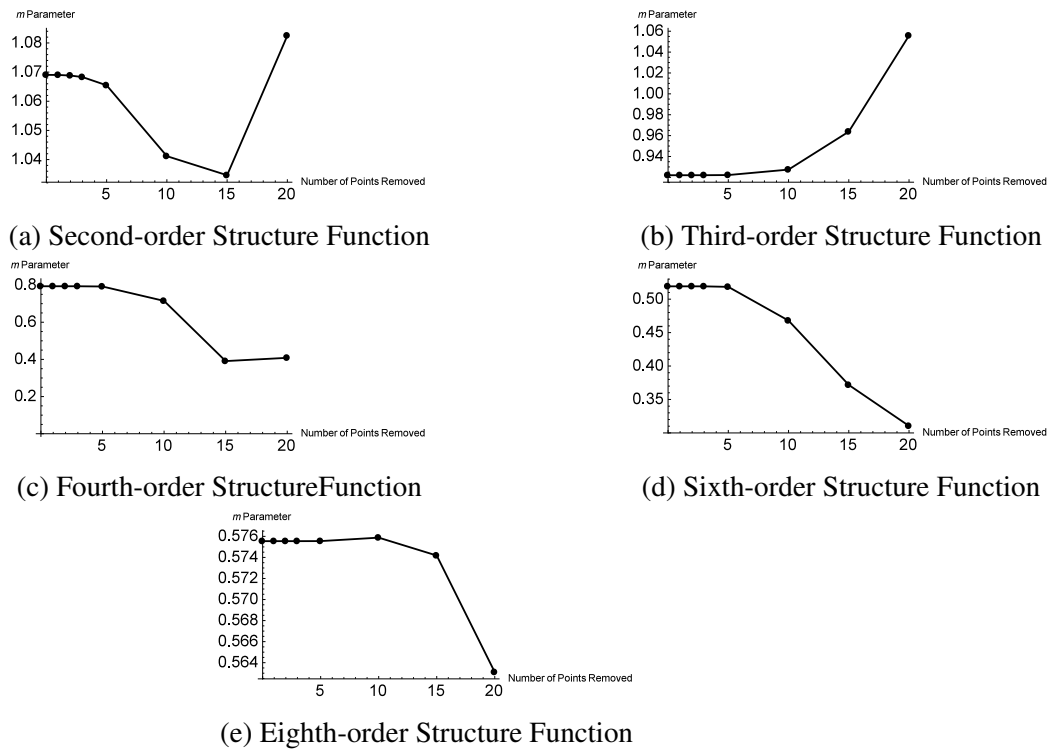(e) Eighth-order Structure Function

Figure 9: Robustness test for a Reynolds number of 508. Note that the x-axis is the number of data points removed from the fitting. We see very little change in the *m* parameter until we remove enough data points to eliminate the dissipative range completely. Note the scales on the y-axis. As a result, we are convinced our fits are not dependent on the probe size.
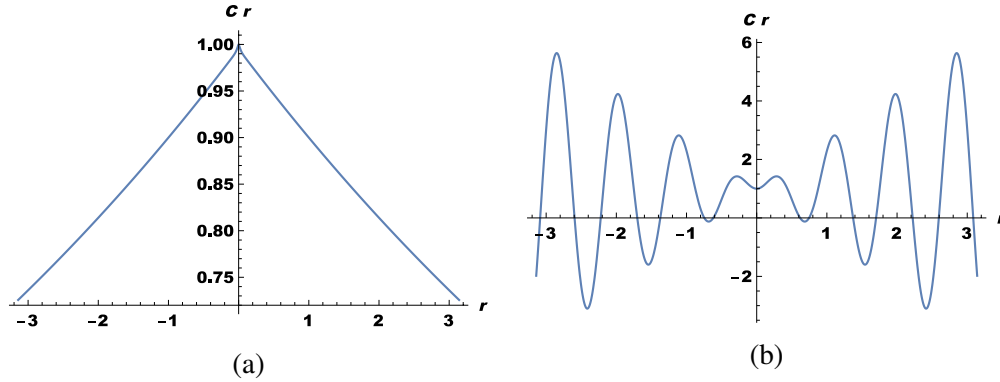
Figure 10: (a) The normalized (Pearson's coefficient) two point correlation, of the noise in the Navier-Stokes equation (25), for Taylor-Reynolds number 110, with values of a and b from the first line in Table 5, and C from the first column, first line of Table 4.
(b) The normalized (Pearson's coefficient) two point correlation, of the noise in the Navier-Stokes equation (25), for Taylor-Reynolds number 1450, with values of a and b from the last line in Table 5, and C from the last column, first line of Table 4.

stochastic Navier-Stokes equation (7). Recall that the original conjecture by Landau and Lifschitz [20] was that the noise was white or uncorrelated. The question can be rephrased to ask what the noise forcing is that the fluid velocity is subjected to in fully developed turbulence. In the stochastic Navier-Stokes equation the noise was modeled (SCT) as a Fourier series with infinitely many coefficients, but now these coefficients have been determined by the experimental data in Section 5. The following observations can be made:

The Noise in Homogeneous Turbulence:

1. The color of the noise, in the stochastic Navier-Stokes equation (7) depends on the Reynolds number through the coefficients a, b and the exponent m.

2. For small Reynolds number the mean-field noise, or the central limit theorem and large deviation noise, is exponentially correlated (decaying), with correlation:
$$C_r = \frac{C}{2}e^{-2\pi br} + \frac{1}{2}e^{-2\pi ar}(r + \frac{1}{2\pi a}),$$

33

up to a multiplicative factor of $\frac{1}{C^2}$, where the values of $b(Re_\lambda)$ (central limit theorem), $a(Re_\lambda)$ (large deviation), and $m(Re_\lambda)$ (spatial smoothness) are taken from Tables 4, 5 and 6, for low values of Re_λ, and $r = |x - y|$ is the correlation distance between two points x and y in the fluid, see Figure 10a.

3. For large Reynolds number the mean-field noise become oscillatory, approaching the correlation:

$$C_r = \frac{C}{2} b \cos(2\pi b^2 r) + 2\pi a^2 r \sin(2\pi a^2 r),$$

up to a multiplicative factor of $\frac{1}{C^2}$, again taking the values from Tables 4, 5 and 6, for high values of Re_λ, see Figure 10b.

These correlations are computed using the variance of the velocity and the second-order structure function above, using the well-known formula $S_2(r) = 2(\sigma - C_r)$ and taking the limit of a very large spatial period. The exact formulas of the correlations depend on the ansatz that we made for the coefficients c_k and d_k in Section 4.1, but the above statements, about the nature of the correlations, are true in general.

Once we put in the values of b and a from Table 5, we see that the slow decay of e^{-br} (central limit theorem) dominates for small Reynolds numbers, but the rapid oscillations of $\sin(a^2 r)$ (large deviation) dominate for large Reynolds number. Recall, however, that these are the correlations of the noise in the stochastic Navier-Stokes equation, not the correlations of the turbulent velocity itself, see section 7.

8   Sensitivity Analysis

Now that we have compared the experimental data from the VDTT to formulas computed by the SCT, it is desirable to check how robust these results are. In particular, we want to know if the formulas with the Reynolds number corrections do better than the formulas without them? Also do the results depend on the probe size used in the experiments or are they independent of it? In this section we perform a sensitivity analysis to test the results and answer these questions.

First we consider the formula for the general p-th structure function as given in (21). One way to let the Reynolds Number go to infinity is to let the viscosity of the fluid go to zero. Doing so simplifies the coefficients A_p in (20), so that for

34

Taylor Reynolds Number	110	264	508	1000	1450
Second	2.09081	1.49402	1.31448	1.07963	0.984291
Third	1.79012	1.41339	1.05553	0.822192	0.730565
Fourth	1.6408	1.09179	0.920749	0.687336	0.595942
Sixth	1.65727	1.08667	0.91658	0.681818	0.592901
Eighth	1.66164	1.06728	0.901549	0.662111	0.577724

Table 7: The fitted values for m for the uncorrected for Reynolds number effects structure function fits

$R_\lambda = \infty$, $\nu = 0$,

$$A_p = \frac{2^{\frac{p}{2}}\Gamma(\frac{p+1}{2})\sigma_k^p {}_1F_1(-\frac{1}{2}p, \frac{1}{2}, -\frac{1}{2}(\frac{M_k}{\sigma_k})^2)}{|k|^{\zeta_p}}. \tag{26}$$

The further denominator terms found in (26) but not above are corrections to the formula to account for the Reynolds number of the flow. Data fits were also done to the formula without the Reynolds number corrections. Figures 11, 12, 13, 14, and 15 are plots of the error between the formula fits and the data at each data point. The blue circles are the error to the Reynolds corrected formulas while the red diamonds are the error to the formula without the Reynolds number correction.

There are a couple of observations to make about the error plot. First, for small Taylor Reynolds numbers, it appears that the corrections improve the fitting, especially for the smaller data points. This improvement erodes as the Taylor Reynolds number increases, until we see very little difference in accuracy for Taylor Reynolds number 1450. This makes sense, as the corrections to account for Reynolds number get smaller as the Reynolds number increases, with the formulas becoming the uncorrected version when we let the Reynolds number go to infinity.

We also see an issue in fitting the smallest data points for solely for Reynolds Number 1450. This issue appears to be connected to the system length, as seen in Figure 7. A second fit to the fourth structure function for this Reynolds number was found with $D = .921$. This does improve the fitting for the smaller data points. However, D being this small causes an issue at the larger data points, namely the sine curve wants to return to zero before the last data point. Since there are relatively few data points at small values of r/η, we set $D = 1.3$. The value of 1.3 was chosen as it the smallest number needed to fully capture the larger data
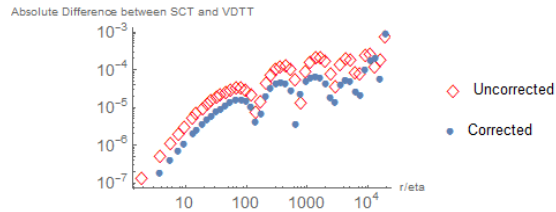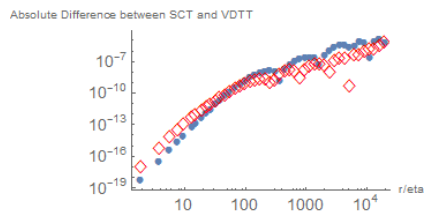
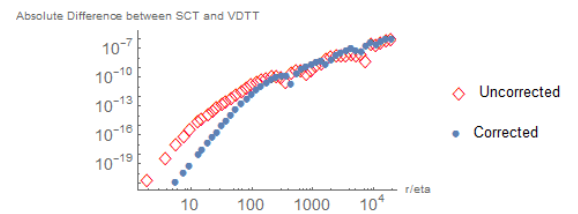(a) Second-Order Structure Function Error
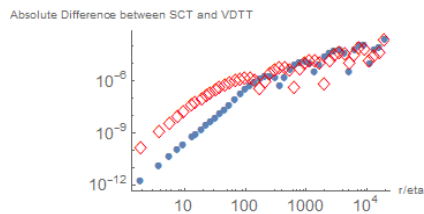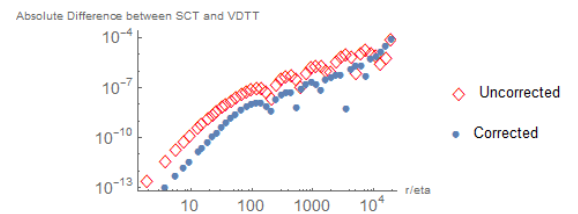
(b) Third-Order Structure Function Error

(c) Fourth-Order Structure Function Error

(d) Sixth-Order Structure Function Error

(e) Eighth-Order Structure Function Error

Figure 11: Error for Taylor Reynolds Number 110. Note that the plots are made on a log-log scale. The blue dots are fits to the structure function formula featuring the Reynolds correction whereas the red diamonds are fits to the structure function formula without the Reynolds number correction

36

(a) Second-Order Structure Function Error

(b) Third-Order Structure Function Error

(c) Fourth-Order Structure Function Error

(d) Sixth-Order Structure Function Error
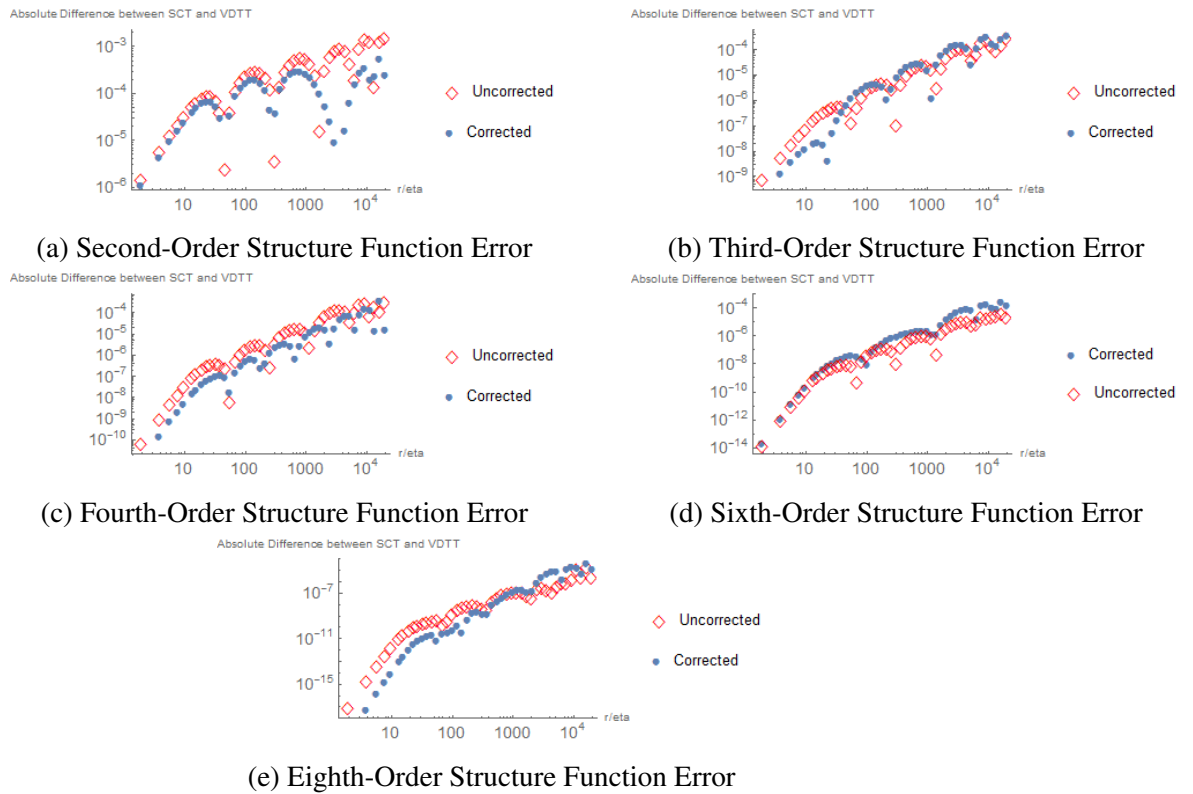
(e) Eighth-Order Structure Function Error

Figure 12: Error for Taylor Reynolds Number 264. Note that the plots are made on a log-log scale. The blue dots are fits to the structure function formula featuring the Reynolds correction whereas the red diamonds are fits to the structure function formula without the Reynolds number correction

37

(a) Second-Order Structure Function Error

(b) Third-Order Structure Function Error

(c) Fourth-Order Structure Function Error

(d) Sixth-Order Structure Function Error
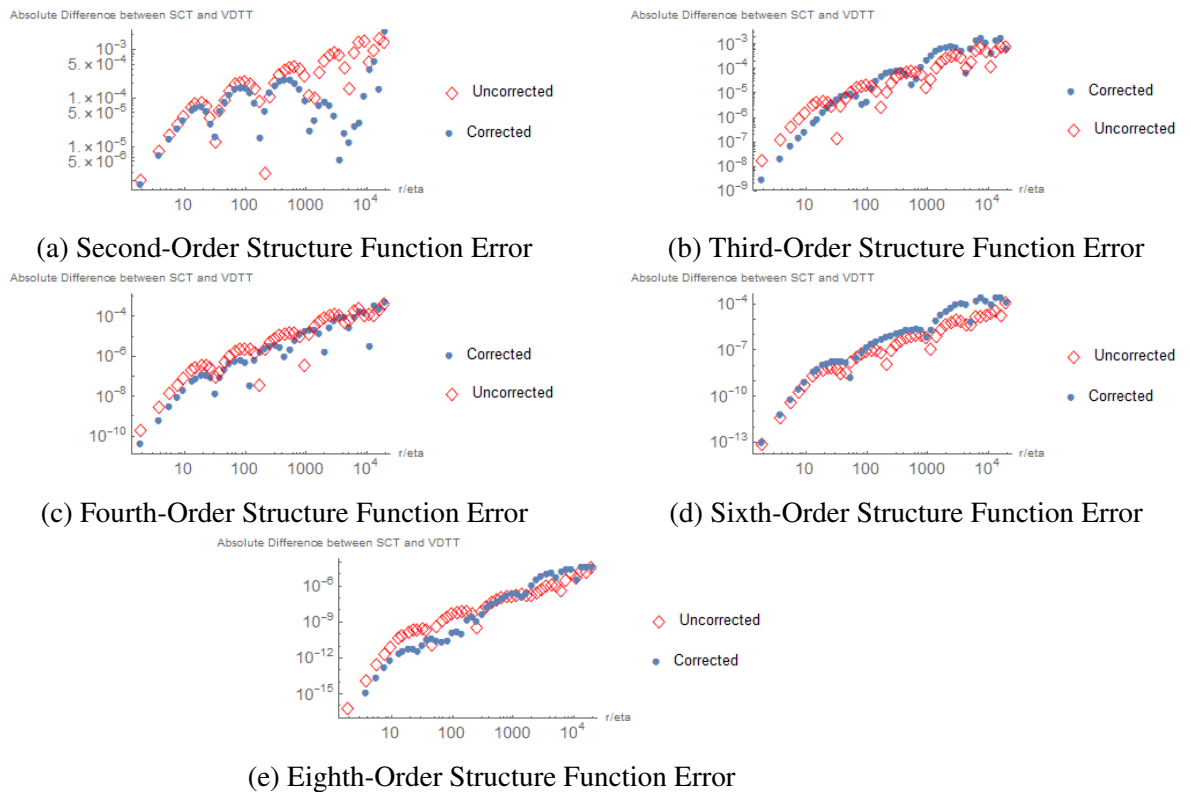

(e) Eighth-Order Structure Function Error

Figure 13: Error for Taylor Reynolds Number 508. Note that the plots are made on a log-log scale. The blue dots are fits to the structure function formula featuring the Reynolds correction whereas the red diamonds are fits to the structure function formula without the Reynolds number correction.
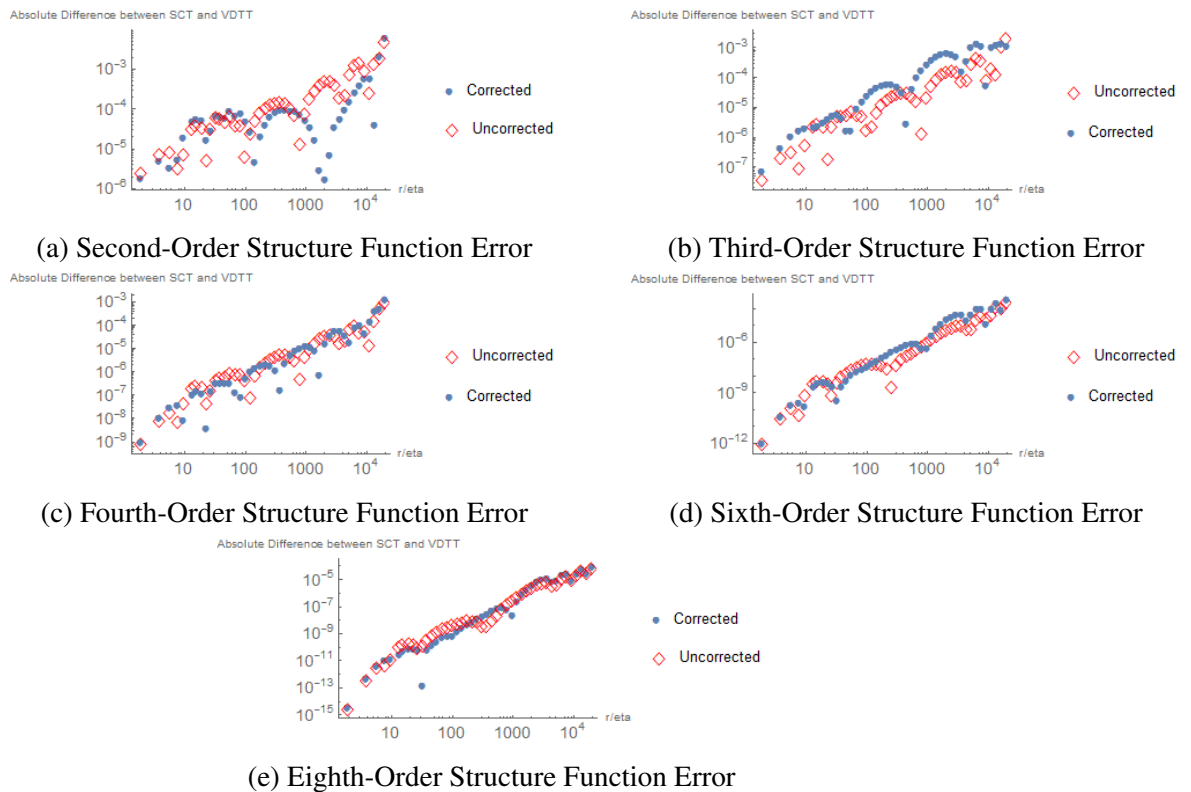
(a) Second-Order Structure Function Error

(b) Third-Order Structure Function Error

(c) Fourth-Order Structure Function Error

(d) Sixth-Order Structure Function Error

(e) Eighth-Order Structure Function Error

Figure 14: Error for Taylor Reynolds Number 1000. Note that the plots are made on a log-log scale. The blue dots are fits to the structure function formula featuring the Reynolds correction whereas the red diamonds are fits to the structure function formula without the Reynolds number correction.
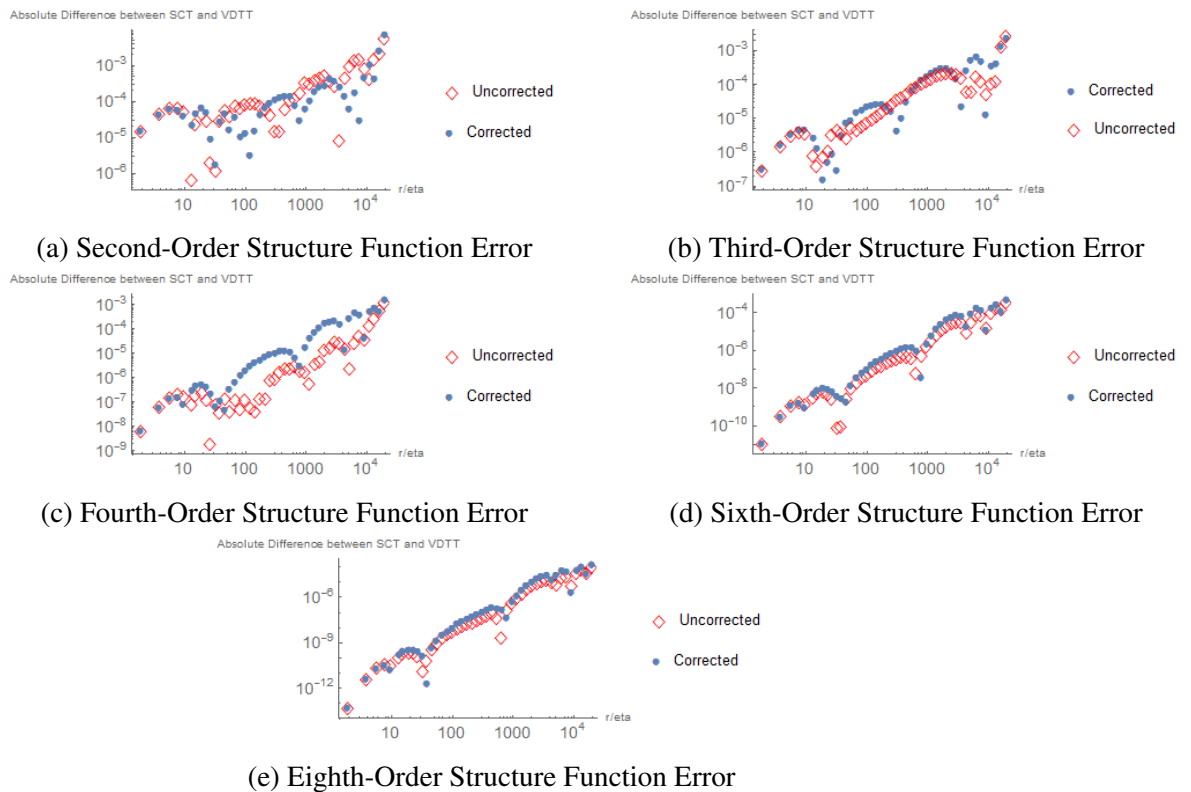
(a) Second-Order Structure Function Error

(b) Third-Order Structure Function Error

(c) Fourth-Order Structure Function Error

(d) Sixth-Order Structure Function Error

(e) Eighth-Order Structure Function Error

Figure 15: Error for Taylor Reynolds Number 1450. Note that the plots are made on a log-log scale. The blue dots are fits to the structure function formula featuring the Reynolds correction whereas the red diamonds are fits to the structure function formula without the Reynolds number correction.
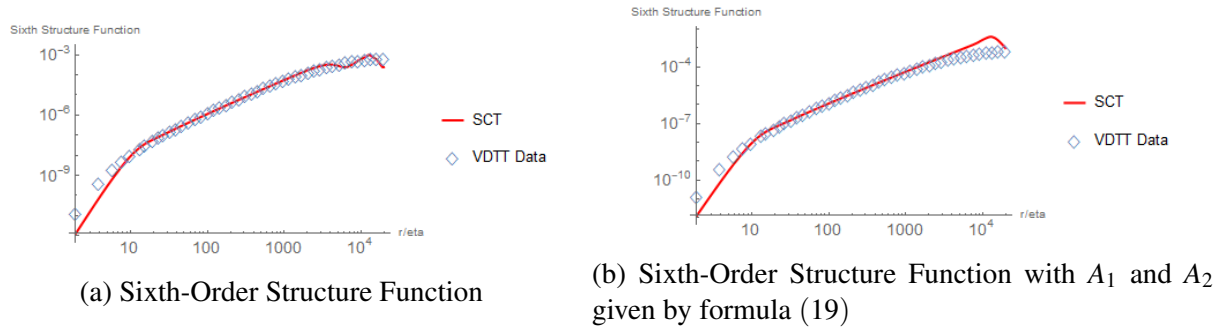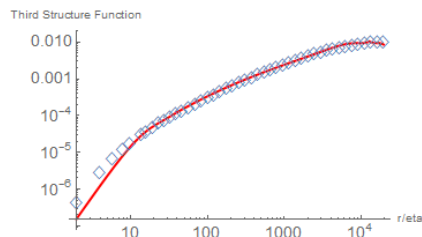
(a) Sixth-Order Structure Function

(b) Sixth-Order Structure Function with A_1 and A_2 given by formula (19)

Figure 16: The figure on the left is the original fit to the sixth-order structure function for Reynolds number 1450. The right is if we tie A_1 and A_2 back to the original formula (19). Note the effect on the largest values of r/η and how this creates the wiggles we are seeing.

points. Figure 7 also illustrates the effect D has on the fits, serving to place the transition from the dissipative range into the inertial range.

One potential point of concern with the fitting result was the probe size. The size of the probe could influence the fit and a different probe size could produce different result. To check for this, fits were redone with a reduced number of data points. In particular, for every Taylor Reynolds number and every structure function, fits were redone without including the first, the first two, and the first three data points respectively. We saw minimal change in the main parameters. the greatest being a difference of one in the third significant digit. The robust test for Reynolds Number 508 are included in figure 9. As we can see, there is not a significant change in the value of m when removing the first couple of data points. However, the removal of fifteen or more data points removes the entire dissipative range and so we would expect the changes to be significant. As a result, we are convinced the fits are unaffected by the probe size.

Finally, we show the effect parameters A_1, A_2, and C have on the fits. Figure 16 shows the effects of A_1 and A_2. Note that these effects show up for all Reynolds number and all order of structure functions, although they become negligible as the order of the structure function increases. These two parameters also created the wiggles we see at the largest values of r/η. Figure 17 shows the effect of parameter C. This parameter places the vertical location of the transition out of the inertial range.

(a) Third-Order Structure Function
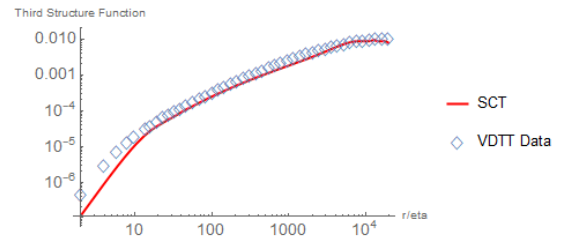
(b) Third-Order Structure Function Error with slight change in parameter C.
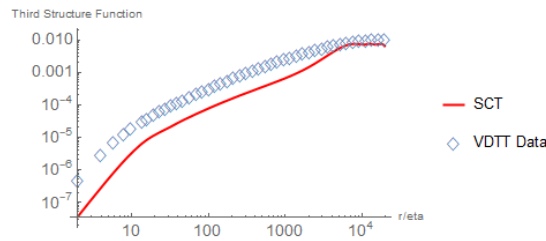
(c) Third-Order Structure Function with a greater change in parameter C.

Figure 17: The figure on the top left is the original fit to the third-order structure function for Reynolds number 1450. The top right changes the value of the parameter C from 3.59 to 4. Note the effect here, as the original fit for the dissipative and inertial range are pushed down slightly, and a new transitionary regime is created. This effect is more pronounced in the bottom figure, when C is increased from 4 to 6.

9 Conclusion

We started by following Kolmogorov's method as described in Section 2 to close the Navier Stokes equations that describe fully developed turbulence. We did this by introducing a stochastic forcing term to account for the small scales, see [6]. Having closed the model, we then compute a sine series representation for the structure functions of turbulence, with Reynolds number corrections. These formulas were then fitted to data generated from the Variable Density Turbulence Tunnel at the Max Planck Institute for Dynamics and Self-Organization. The fits proved to be good with seven parameters. However, only three of these parameters a, b, m were active over the entire range of T-R numbers in the experiment, although one more parameter C measures the mean fluctuation velocity and increases over the range of T-R numbers in the experiment. Of the other four D, A_1, A_2 and C, one D is active only for the transition from the dissipative range into the inertial range, whereas the other three are active for the transition out of the inertial range.

We also compared fits to the formula with a correction to account for the Reynolds number to fits without that correction. We see that the Reynolds correction formulas generate better fits as the Reynolds number increases for lower structure functions but have little impact on the fits for the higher structure functions.

10 Acknowledgements

References

[1] John D Anderson Jr. *A history of aerodynamics: and its impact on flying machines*, volume 8. Cambridge University Press, 1999.

[2] Donald D Baals and William R Corliss. *Wind tunnels of NASA*, volume 440. Scientific and Technical Information Branch, National Aeronautics and Space Administration, 1981.

[3] O. E. Barndorff-Nilsen. Exponentially decreasing distributions for the logarithm of the particle size. *Proc. R. Soc. London*, A 353:401–419, 1977.

[4] P. S. Bernard and J. M. Wallace. *Turbulent Flow*. John Wiley & Sons, Hoboken, NJ, 2002.

[5] R. Bhattacharya and E. C. Waymire. *Stochastic Processes with Application*. John Wiley, New York, 1990.

[6] B. Birnir. The Kolmogorov-Obukhov statistical theory of turbulence. *J. Nonlinear Sci.*, 2013. DOI 10.1007/s00332-012-9164-z.

[7] B. Birnir. *The Kolmogorov-Obukhov Theory of Turbulence*. Springer, New York, 2013.

[8] Björn Birnir. *From Wind-Blown Sand to Turbulence and Back*, pages 15–27. Springer International Publishing, Cham, 2016.

[9] Daniel B. Blum, Gregory P. Bewley, Eberhard Bodenschatz, Mathieu Gibert, Armann Gylfason, Laurent Mydlarski, Greg A. Voth, Haitao Xu, and P.K. Yeung. Signatures of non-universal large scales in conditional structure functions from various turbulent flows. *New Journal of Physics*, 13:113020, 2011.

[10] Eberhard Bodenschatz, Gregory P Bewley, Holger Nobach, Michael Sinhuber, and Haitao Xu. Variable density turbulence tunnel facility. *Review of Scientific Instruments*, 85(9):093908, 2014.

[11] Genevieve Comte-Bellot and Stanley Corrsin. The use of a contraction to improve the isotropy of grid-generated turbulence. *Journal of Fluid Mechanics*, 25(04):657–682, 1966.

[12] S Corrsin. Turbulent flow. *American Scientist*, 49(3):300–325, 1961.

[13] Giuseppe Da Prato and Jerzy Zabczyk. *Encyclopedia of Mathematics and its Applications: Stochastic Equations in Infinite Dimensions*. Cambridge University Press, 2014.

[14] B. Dubrulle. Intermittency in fully developed turbulence: in log-Poisson statistics and generalized scale covariance. *Phys. Rev. Letters*, 73(7):959–962, 1994.

[15] Geoffrey Grimmett and David Stirzaker. *Probability and Random Processes*. 3 edition.

[16] B.R. Hunt, T. Sauer, and J.A. Yorke. Prevalence: A translation-invariant "almost every" on ininite-dimensional spaces. *Bull. of the Am. Math. Soc.*, 27(2):217–238, 1992.

[17] A. N. Kolmogorov. Dissipation of energy under locally istotropic turbulence. *Dokl. Akad. Nauk SSSR*, 32:16–18, 1941.

[18] A. N. Kolmogorov. The local structure of turbulence in incompressible viscous fluid for very large Reynolds number. *Dokl. Akad. Nauk SSSR*, 30:9–13, 1941.

[19] A. N. Kolmogorov. A refinement of previous hypotheses concerning the local structure of turbulence in a viscous incompressible fluid at high Reynolds number. *J. Fluid Mech.*, 13:82–85, 1962.

[20] Lev Davidovich Landau and Evgenii Mikhailovich Lifshits. *Fluid Mechanics: Transl. from the Russian by JB Sykes and WH Reid*. Addison-Wesley, 1959.

[21] C.B. Millikan, J.E. Smith, and R.W. Bell. High-speed testing in the southern california cooperative wind tunnel. *Journal of the Aeronautical Sciences*, 15(2):69–88, 1948.

[22] B. Oksendal. *Stochastic Differential Equations*. Springer, New York, 1998.

[23] S. B. Pope. *Turbulent Flows*. Cambridge Univ. Press, Cambridge UK, 2000.

[24] Ludwig Prandtl. Göttingen wind tunnel for testing aircraft models, 1920.

[25] O. Reynolds. On the dynamical theory of incompressible viscous fluids and the determination of the criterion. *Phil. Trans. Roy. Soc. Lond.*, 186A:123–164, 1885.

[26] Z-S She and E. Leveque. Universal scaling laws in fully developed turbulence. *Phys. Rev. Letters*, 72(3):336–339, 1994.

[27] Z-S She and E. Waymire. Quantized energy cascade and log-poisson statistics in fully developed turbulence. *Phys. Rev. Letters*, 74(2):262–265, 1995.

[28] Michael Sinhuber, Gregory P. Bewley, and Eberhard Bodenschatz. Dissipative effects on inertial-range statistics at high reynolds numbers. *Physical Review Letters*, 119:134502, 2017.

[29] Michael Sinhuber, Eberhard Bodenschatz, and Gregory P. Bewley. Decay of turbulence at high reynolds numbers. *Physical Review Letters*, 114:034501, 2015.

[30] G. I. Taylor. Statistical theory of turbulence. *Proc. Royal Soc. London*, 151:421–444, 1935.

[31] Margit Vallikivi and Alexander J. Smits. Fabrication and characterization of a novel nanoscale thermal anemometry probe. *Journal of Microelctromechanical Systems*, 23, 2014.

[32] J. B. Walsh. *An Introduction to Stochastic Differential Equations*. Springer Lecture Notes, eds. A. Dold and B. Eckmann, Springer, New York, 1984.